TECHNICAL REPORT No. 55

FINITE ELEMENT SCHEMES FOR THE VERTICAL DISCRETISATION OF THE ECMWF FORECAST MODEL USING QUADRATIC AND CUBIC ELEMENTS

by

J. Steppeler

February 1986

Abstract

Finite element schemes with second and third order basis functions are introduced for a σ-coordinate version of the ECMWF spectral model. The basis functions are required to be continuous for the second order case, and have continuous first and second derivatives for the third order splines.

The performance of these schemes was investigated by a series of test forecasts, which resulted in an improved forecast skill for the finite element schemes. 50 day integrations showed a substantial impact of the discretization on the model climate, in accordance with Burridge et al. (1985)

A data assimilation experiment showed that after only 12 hours there was a reduction of the first guess error with the cubic spline scheme.

CONTENTS

1. INTRODUCTION

The numerical accuracy of horizontal approximations in numerical weather prediction models has improved noticeably due to the development of the spectral method. In comparison, vertical discretization techniques are much less developed. Most models in use today are based on centred differences, which are second order accurate only on regular grids.

The models developed by Staniforth et al. (1977) and Burridge et al. (1985) use linear finite element basis functions for vertical discretization. For regular grids these methods have an accuracy comparable to that of the fourth order Kreiss-Oliger (1972) method.

This investigation goes a step further by introducing into a sigma coordinate version of the ECMWF spectral model basis functions of order 2 and 3 for the Galerkin finite element (FE) treatment of the vertical discretisation. Such schemes have a numerical accuracy which approximately matches that of the spectral method, evaluated for the linear advection equation (Gallagher, 1978; Steppeler, 1976b). Furthermore, the cubic spline elements are expected to have a high numerical accuracy for all scales even on irregular grids. Even if no superconvergence occurs, the scheme will be at least third order.

A potential problem with finite elements is the existence of computational modes; they were encountered by Staniforth et al. (1977). In particular the high accuracy of the second order elements is achieved at the cost of a rather poor representation of the smallest scales (Steppeler, 1976a), which might increase the problems with the computational modes. This problem can also exist for the spectral method when dealing with non-linear terms. In this case, the problem is overcome by filtering a part of the spectrum.

Successful implementation of second and third order FE-schemes for horizontal discretization has been achieved by introducing a selective damping of the computational modes (Steppeler, 1976a).

The use of a numerical method for vertical discretization is quite a distinct problem from that for horizontal discretization. Vertical diffusion is usually included in models to represent the corresponding physical effect, but it is not a numerical necessity. Therefore it is desirable that the FE-scheme works without filtering. For the methods described here this was investigated by examining vertical cross-sections of the temperature field. The second and third order method did not suffer any apparent problems with computational modes.

For horizontal resolution, it is appropriate to introduce approximations in addition to the Galerkin approximation to obtain a scheme which is computationally cheap. For example, Steppeler (1976b) neglected terms of high order in Δx and a simplified Galerkin procedure was used. In contrast, for vertical discretization we use only the Galerkin procedure because in this way we can obtain the following: energy conservation, a higher accuracy than with additional approximations, and for one space-dimension the straightforward Galerkin procedure is reasonably cheap computationally.

The technical aspects of implementing the scheme differ substantially according to the continuity requirements imposed on the basis functions. Requiring just continuity for second order elements, as in Steppeler (1976b), results in a relatively simple scheme, which will be approximately as expensive as the first order elements. This simplicity is achieved because the second order field representation is obtained by adding to a first order scheme one basis function which has support in only one grid interval

$(\sigma_\nu, \sigma_{\nu+1})$. Since the expense of a scheme depends very much on the degree of overlapping of the basis functions, this advantage partly offsets the complications caused by the increased order.

In this study we assume that the second order element-functions are continuous. Computational efficiency is obtained by applying transformations to appropriate basis-functions, as will be described in Section 3.1.

The cubic splines are assumed to be continuous, and have continuous first and second derivatives. Therefore each basic spline overlaps four intervals. One way of obtaining computational efficiency with this scheme is to transform to a collocation grid as described in Section 3.2.

Previous experience with linear finite elements indicated that some care in approximating the top boundary element is essential. In this study a relatively sophisticated boundary treatment, the B4-treatment of Burridge et al. (1985), is only used with the quadratic elements. The cubic spline scheme uses a simplified treatment obtained by extending the least square approximation integrals only to $\sigma=\sigma_1$. A more appropriate treatment of this boundary is left until the development of a hybrid coordinate version of this model.

Section 4.1 reports the result of a data assimilation experiment and Section 4.2 gives the result of a series of 10 day forecasts. Section 4.3 describes the longer range behaviour of FE-models using 50 day integrations.

2. GALERKIN PROCEDURE

Galerkin discretizations for a σ-coordinate model are based on functional representations for a field $\phi(\sigma)$ of the form:

$$\phi(\sigma) = \sum_{\nu=1}^{NLEV} \phi_\nu^A \, b_\nu(\sigma) \qquad (1)$$

The basis functions $b_\nu(\sigma)$ which determine the method are defined in Section 3. Other than for the linear splines used by Burridge et al. (1985), the amplitudes ϕ_ν^A are no longer node point values of the field $\phi(\sigma)$, since when the order is greater than one, the b_ν are different from 0 at more than one node point.

When computing the right hand side of the dynamic equations with functions of the form (1), the result cannot be represented by (1). Such functions are mapped to fields representable by (1) by Galerkin operations G, as pointed out in more detail by Burridge et al. (1985). Different Galerkin operations G_1, G_2 are possible for different sets of basis functions b_ν in (1). For example, in Burridge et al. (1985) two sets of basis functions with respect to boundary elements are used. The first interpolates to 0 in the top and bottom intervals, whereas the second has piecewise constant elements there. The Galerkin method is only used for the adiabatic part of the model; the physical parameterisation is done in node point space, as in the operational ECMWF model.

An energy conserving Galerkin procedure for the adiabatic part of the dynamic equations was formulated by Burridge et al. (1985) for a rather wide class of basis functions. The equations are stated here in a slightly different form (see Louis, 1984), but for an appropriate horizontal spectral truncation they are equivalent.

$$\frac{\partial u}{\partial t} - G_1[(f+\xi)v+\dot{\sigma}\frac{\partial u}{\partial \sigma} + \frac{R\tilde{\tilde{T}}}{a}\frac{\partial \ell np_s}{\partial \lambda} + \frac{1}{a}\frac{\partial}{\partial \lambda}(\tilde{\phi}+E)]=0$$

$$\frac{\partial v}{\partial t} + G_1[(f+\xi)u+\dot{\sigma}\frac{\partial v}{\partial \sigma} + \frac{R\tilde{\tilde{T}}}{a}(1-\mu^2)\frac{\partial \ell np_s}{\partial \mu} + \frac{(1-\mu^2)}{a}\frac{\partial}{\partial \mu}(\tilde{\phi}+E]=0$$

$$\frac{\partial T}{\partial t} + G_2[\frac{u}{a(1-\mu^2)}\frac{\partial T}{\partial \lambda} + \frac{v}{a}\frac{\partial T}{\partial \mu} + \dot{\sigma}\frac{\partial T}{\partial \sigma} - \frac{K}{p_s\sigma}(\tilde{T}\omega_1+\tilde{\tilde{T}}\omega_2)]=0 \qquad (2)$$

$$\tilde{\phi}_\sigma = -\frac{R\tilde{T}}{\sigma}$$

$$\omega_1 = p_s\dot{\sigma} + \sigma\dot{p}_s \text{ and } \omega_2 = \sigma\,\underline{v}.\nabla p_s$$

$$\dot{\sigma} = 0 \text{ for } \sigma = 0,1$$

$$\frac{\partial}{\partial t}\ell np_s + \nabla.\underline{v} + \underline{v}.\nabla\ell np_s + \frac{1}{p_s}\frac{\partial}{\partial \sigma}(p_s\dot{\sigma})$$

In (2), no approximating operators appear in the diagnostic equations for ϕ, $\dot{\sigma}$, ω_1 and ω_2, so these equations have to be evaluated exactly. $\tilde{T}$ and $\tilde{\tilde{T}}$ can be interpolated from T in a rather arbitrary way, not necessarily by a Galerkin operation. Here we define $\tilde{T}$ and $\tilde{\tilde{T}}$ to be the virtual temperature for $\sigma \in (\sigma_1, \sigma_{NLEV})$. Only for the top and bottom intervals do we use different choices for $\tilde{T}$, which define various options for the boundary treatment. Since we use always linear interpolation for the top and bottom intervals, and high order interpolation only for the middle intervals, we can immediately take over the boundary options B0...B4 from Burridge et al. (1985). The results obtained indicate that the development of appropriate approximations near the top boundary can be very effective in increasing the forecast skill. However, most of the experiments reported here use a boundary treatment in which the dynamic equations in the top interval $(0, \sigma_1)$ are not approximated. This simplified model is obtained by extending the integral in (3) only from σ_1 to 1.

For the moist equations, $\tilde{T}$ will be the virtual temperature which is computed at node points, and the appropriate interpolation assumption according to (1) is made. Furthermore K in the thermodynamic equation is moisture dependent; this is also evaluated in node point space.

3. FIELD REPRESENTATIONS, BASIS-FUNCTIONS AND TRANSFORMATIONS

The basis representation of the field ϕ is by node point-values ϕ_ν, $\nu \in \{1, \ldots, \text{NLEV}\}$. This representation is necessary so as to have an interface to the physics routines. The transformation to the amplitudes ϕ^A_ν of (1) will be given in this section. Note that there is a one to one correspondence between ϕ_ν and ϕ^A_ν.

Since the finite element method is Galerkin based, it has many features in common with the spectral method. Both the representations ϕ_ν and ϕ^A_ν are analogous to the representations in spectral space.

The Galerkin operation G applied to some function $\phi(\sigma)$, is defined to be a function $\breve{\phi}(\sigma)$ of the form given by (1). The coefficients $\breve{\phi}_\nu$, belonging to $\breve{\phi}(\sigma)$ according to (1), are defined by

$$\int_0^1 [(\sum_{\nu=1}^{\text{NLEV}} \breve{\phi}_\nu \, b_\nu(\sigma)) - \phi(\sigma)] b_\mu(\sigma) d\sigma = 0 \qquad \mu = 1, \ldots \text{NLEV} \qquad (3)$$

An important step for the implementation of a Galerkin method is the computation of the Galerkin integrals $\int b_\mu(\sigma) f(\sigma) d\sigma$, with f being the right-hand side of the equations. This is explained in more detail in Section 2 of Burridge et al. (1985).

For the spectral method, an efficient method of computing the Galerkin integrals is by the introduction of a collocation grid ϕ^C_ν, $\nu \in \{1, \ldots, \text{NCOL}\}$. The same is also possible with finite elements. However there is no one to one correspondence between ϕ_ν and ϕ^C_ν, the collocation grid having much more resolution than the node point grid.

Various technical aspects associated with the collocation grid will be discussed in this section.

Unlike the spectral method, the finite element scheme uses localised basis functions. This allows as an alternative the direct computation of the Galerkin integrals. In fact, so far this has been the most common method used, and was employed by Burridge et al. (1985). For higher order basis functions, it is desirable to find the most efficient direct method. A tool to achieve efficiency is the use of different basis function representations, alternative to that given in (1). In this section, transformations to such representations will be given.

We confine this presentation to the σ-system in which all fields are represented on levels

$$\sigma_\nu, \quad \nu \in \{1,.....,NLEV\} \tag{4}$$

In order to avoid additional complications, this presentation excludes staggered grids.

3.1 Second order elements

(a) Representation of fields as linear splines plus a quadratic correction

We allow the possibility of representing only the middle atmosphere by second order elements, keeping a first order representation for the rest of the atmosphere. Let ν_B, ν_T be the levels between which the fields are to be represented by second order elements. It is required that

$$\nu_B - \nu_T = 2r \qquad r \in \{1,2.....\} \tag{5}$$

There will be r-1 nodepoints for the linear spline between ν_B and ν_T, and r points to define a quadratic correction (see Fig. 1).

It is evident from Fig. 1 that the introduction of a quadratic spline is appropriate for models requiring very good resolution in the middle atmosphere.

Basis functions h_ν for the quadratic correction are associated with odd values of $\nu-\nu_B$, $\nu \in (\nu_B,\nu_T)$. For the other ν linear basis functions e_ν are defined. The range of ν to define h_ν will be called H, and the range of ν for the definition of e_ν will be called F.

The basis functions for the linear part of the field are the same as used with a linear FE-method (see Fig. 1).

$$e_\nu = \begin{cases} (\sigma_{T_\nu}-\sigma)/(\sigma_{T_\nu}-\sigma_\nu) & \text{for } \sigma \in (\sigma_\nu,\sigma_{T_\nu}) \\ (\sigma-\sigma_{B_\nu})/(\sigma_\nu-\sigma_{B_\nu}) & \text{for } \sigma \in (\sigma_{B_\nu},\sigma_\nu) \\ 0 & \text{otherwise} \end{cases} \qquad (6)$$

with

$$\sigma_{B_\nu} = \begin{cases} \sigma_{\nu-2} & \text{if } \nu-2 \geq \nu_B \\ \sigma_{\nu-1} & \text{otherwise} \end{cases}$$

$$\sigma_{T_\nu} = \begin{cases} \sigma_{\nu+2} & \text{if } \nu+2 \leq \nu_T \\ \sigma_{\nu+1} & \text{otherwise} \end{cases}$$

$\nu \in F$

The basis functions for the quadratic correction are:

$$h_\nu = \begin{cases} -\tfrac{1}{2}(\sigma-\sigma_{\nu-1})(\sigma_{\nu+1}-\sigma) & \text{for } \sigma \in (\sigma_{\nu-1},\sigma_{\nu+1}) \\ 0 & \text{otherwise} \end{cases} \qquad (7)$$

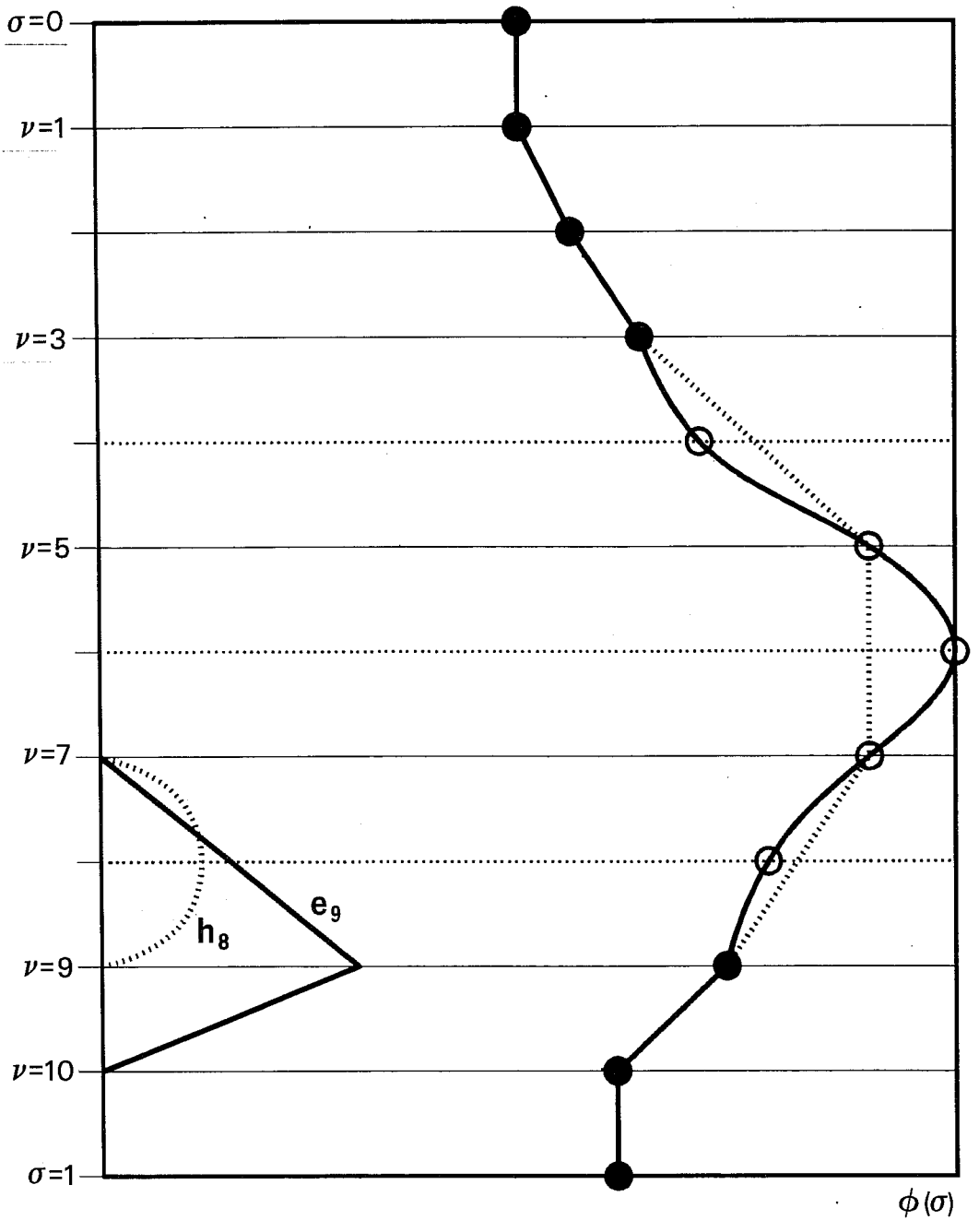

Fig. 1 Representation of the field $\phi(c)$ by quadratic elements for NLEV = 10, $\nu_B = 3$, $\nu_T = 9$, and basis functions e_g and h_g.
o quadratic-correction nodepoints
● nodepoints of the linear spline

The representation of the field is then given by

$$\phi(\sigma)=\sum_{\nu\in F} \phi_\nu e_\nu(\sigma) + \sum_{\nu\in H} \phi_{\sigma\sigma\nu} h_\nu(\sigma) \qquad (8)$$

ϕ^A_ν, $\nu \in F$, and $\phi_{\sigma\sigma\nu}$, $\nu \in H$, are the dynamical variables and provide an equivalent field representation to nodepoint values ϕ_ν, $\nu \in (1, NLEV)$.

(b) Transformation to gridpoint values

This transformation has to be done only for the points $\nu \in H$ determining the quadratic correction, since for the other points $\nu \in F$, ϕ_ν already appears as the amplitude.

Let $\phi_\nu \in (\sigma_{\nu-1}, \sigma_{\nu+1})$ with $\nu \in H$. Then using (8) with $\sigma=\sigma_\nu$, and (6) we obtain

$$\phi_\nu = \frac{\phi_{\nu+1}(\sigma_\nu-\sigma_{\nu-1}) + \phi_{\nu-1}(\sigma_{\nu+1}-\sigma_\nu)}{\sigma_{\nu+1}-\sigma_{\nu-1}} + \phi_{\sigma\sigma_\nu} h_\nu(\sigma_\nu) \qquad (9)$$

(9) is also easily solved for $\phi_{\sigma\sigma_\nu}$. For the formulation of the initial state and to obtain a good interface with the physics routines, it is probably best to choose $\sigma_\nu=\frac{1}{2}(\sigma_{\nu+1}+\sigma_{\nu-1})$ in (9). However, the method will be presented for a general choice of the parameter σ_ν in (9), and the resulting FE-method for the adiabatic part of the model is independent of the choice of σ_ν for $\nu \in H$. The test forecasts will be done using the σ_ν values shown in Fig. 2 (see Section 3.2).

(c) Part orthogonalization

It is appropriate to represent the left-hand sides of the dynamic equations in partly orthogonalized form, because with this basis the matrix inversion in the FE-scheme becomes very simple. We obtain a matrix with two side diagonals for the points $\nu \in F$. This is solved in the same way as for first order elements. For the levels $\nu \in H$ we get an independent set of equations which are diagonal.

The transformations of the basis functions are given by

$$\tilde{e}_\nu = e_\nu + \lambda_{T_\nu} h_{\nu+1} + \lambda_{B_\nu} h_{\nu-1} \tag{10}$$

$$\lambda_{T_\nu} = 0 \quad \text{if } \nu+1 \notin H \tag{11}$$

$$\lambda_{B_\nu} = 0 \quad \text{if } \nu-1 \notin H$$

For the cases not covered by (11), the λ_{T_ν} and λ_{B_ν} are determined by e_ν

$$\lambda_{T_\nu} = -\frac{(e_\nu, h_{\nu+1})}{(h_{\nu+1}, h_{\nu+1})} \tag{12}$$

$$\lambda_{B_\nu} = -\frac{(e_\nu, h_{\nu-1})}{(h_{\nu-1}, h_{\nu-1})}$$

with $(f,g) = \int_0^1 f(\sigma)g(\sigma)d\sigma$.

For (8) the transformation gives (13)

$$\phi(\sigma) = \sum_{\nu \in F} \phi_\nu \tilde{e}_\nu + \sum_{\nu \in F} \tilde{\phi}_\nu h_\nu$$

with

$$\tilde{\phi}_\nu = \phi_{\sigma\sigma_\nu} - \phi_{\nu+1}\lambda_{B_{\nu+1}} - \phi_{\nu-1}\lambda_{T_{\nu-1}} \tag{14}$$

Since $\phi_{\nu+1}$ and $\phi_{\nu-1}$ in (14) are not transformed, (14) can easily be solved for $\phi_{\sigma\sigma_\nu}$.

(d) Transformation to an intermediate basis

In this section we consider transformations concerning a grid interval $(\sigma_{\nu-1}, \sigma_{\nu+1})$, $\nu \in H$, rather than a nodepoint ν.

For the formation of products it may be convenient to transform to the function system

$$\chi_\nu(\sigma) = (\sigma - \sigma_\nu)^\zeta \qquad \zeta \in \{0,1,2\} \text{ and } \nu \in H \tag{15}$$

The reason for this is that the intervals $(\sigma_{\nu-1},\sigma_{\nu+1})$, $\nu \in H$, are those with the minimum overlap of basis functions (i.e. the ones that can represent functions by the least number of basis functions). Therefore it is advantageous to form products first in each interval and then form the scalar products in a second step.

Some of the simplifications achievable in this way are often observed in a more straightforward approach by arithmetic manipulation of the resulting equations.

(e) Transformation to functions with zero main-nodes

Substantial simplifications can be achieved for the formation of products by subtracting a spline which is mapped identically by the Galerkin operation.

For example, the basis function e_ν of (6) normally overlaps 5 other basis functions. The formation of the scalar product of a function e_μ with a product of two functions will in standard form result in 2x5x5 = 50 multiplications. The corresponding operation for a grid-method needs one multiplication.

Let $\nu \in H$ and consider the case when $\nu+1$ and $\nu-1 \in F$. Let a product of $g(\sigma)$ and $f(\sigma)$ be formed. For the interval $(\sigma_{\nu-1}, \sigma_{\nu+1})$ we then form according to Section 3.1(d) the representation:

$$g(\sigma)=g_{\nu-1}+g_{\sigma\sigma_\nu} h_\nu(\sigma) + \tilde{g}_{\nu-1}\cdot(\sigma-\sigma_{\nu-1}) \qquad (16)$$

with $$\tilde{g}_{\nu-1}= \frac{g_{\nu+1}-g_{\nu-1}}{\sigma_{\nu+1}-\sigma_{\nu-1}}$$

$$f(\sigma)=f_{\nu+1}+f_{\sigma\sigma_\nu} h_\nu(\sigma) + \tilde{f}_{\nu+1}\cdot(\sigma-\sigma_{\nu+1}) \qquad (17)$$

with $$\tilde{f}_{\nu+1}= \frac{f_{\nu-1}-f_{\nu+1}}{\sigma_{\nu-1}-\sigma_{\nu+1}}$$

We can write the product in the form:

$$g.f=\alpha^1(\sigma)+\alpha^2(\sigma) \tag{18}$$

$$\begin{aligned}\alpha^1(\sigma)=&g_{\nu-1}f_{\nu+1}+g_{\nu-1}\tilde{f}_{\nu+1}(\sigma-\sigma_{\nu+1})\\&+\tilde{g}_{\nu-1}\cdot(\sigma-\sigma_{\nu-1})f_{\nu+1}+\tilde{g}_{\nu-1}\tilde{f}_{\nu+1}(\sigma-\sigma_{\nu-1})(\sigma-\sigma_{\nu+1})\\&+g_{\nu-1}f_{\sigma\sigma_\nu}h_\nu(\sigma)+f_{\nu+1}g_{\sigma\sigma_\nu}h_\nu(\sigma)\end{aligned}$$

$$\begin{aligned}\alpha^2(\sigma)=&g_{\sigma\sigma_\nu}h_\nu(\sigma).f_{\sigma\sigma_\nu}h_\nu(\sigma)\\&+g_{\sigma\sigma_\nu}h_\nu(\sigma)\tilde{f}_{\nu+1}(\sigma-\sigma_{\nu+1})+f_{\sigma\sigma_\nu}h_\nu(\sigma)\tilde{g}_{\nu-1}(\sigma-\sigma_{\nu-1})\end{aligned} \tag{19}$$

$\alpha^1(\sigma)$ is a quadratic spline and is therefore transformed identically by the Galerkin projection. Using (8) we can obtain $\alpha^1(\sigma)$ by the difference formula

$$\begin{aligned}\alpha^1_{\nu-1}&=g_{\nu-1}f_{\nu-1}\\\alpha^1_{\sigma\sigma_\nu}&=2\tilde{g}_{\nu-1}\tilde{f}_{\nu+1}+g_{\nu-1}f_{\sigma\sigma_\nu}+f_{\nu+1}g_{\sigma\sigma_\nu}\end{aligned} \tag{20}$$

The corresponding spline is given by (8). On average this involves two multiplications per gridpoint. Since (19) involves three linear independent functions per interval, a substantial saving of multiplications is achieved.

Another application is the transformation of a spline to another function system which differs only in the form of the boundary-elements. The formation of the scalar products for this transformation, as done in Burridge et al. (1985), has three multiplications per gridpoint and would require four operations for the quadratic elements. After subtracting the appropriate function, the scalar products are non-zero only for the two boundary elements, so that most of the multiplications can be eliminated.

A special case of function multiplication is that involving the ω-term of the thermodynamic equation. Here it may be particularly useful to transform to zero-node functions because the straightforward formation of scalar products

involves weights which are mostly different from each other. Consequently the possibilities of simplifications by algebraic manipulation are less obvious than for the other products.

3.2 Cubic splines

We use here piece-wise cubic polynomials to interpolate between nodepoints. At nodepoints, continuity of the fields and of their first and second derivatives is required. Fig. 2 gives an example of the cubic spline interpolation on the grid used for the model integrations reported here, and Fig. 3 shows a basis function for the corresponding FE-scheme, overlapping four model intervals.

The idea of using linear interpolation for the top and bottom σ-intervals, which we used with the quadratic splines, is not feasible if we require continuous first and second derivatives also for levels 1 and NLEV. We will therefore not require the continuity of the second derivative for these levels. Another possibility would be to provide four boundary conditions for $\sigma=0$ and $\sigma=1$, which would best be used to define at least two additional boundary related dynamical variables per field.

(a) Interpolation formula

In this section we obtain the polynomial representation of a field defined by its gridpoint values. This can either be used directly to compute the scalar-products of the FE-method or to create fine-mesh data for the collocation approach.

According to Ahlberg (1967) the spline interpolation can be based on the computation of either moments (second derivatives) or first derivatives at

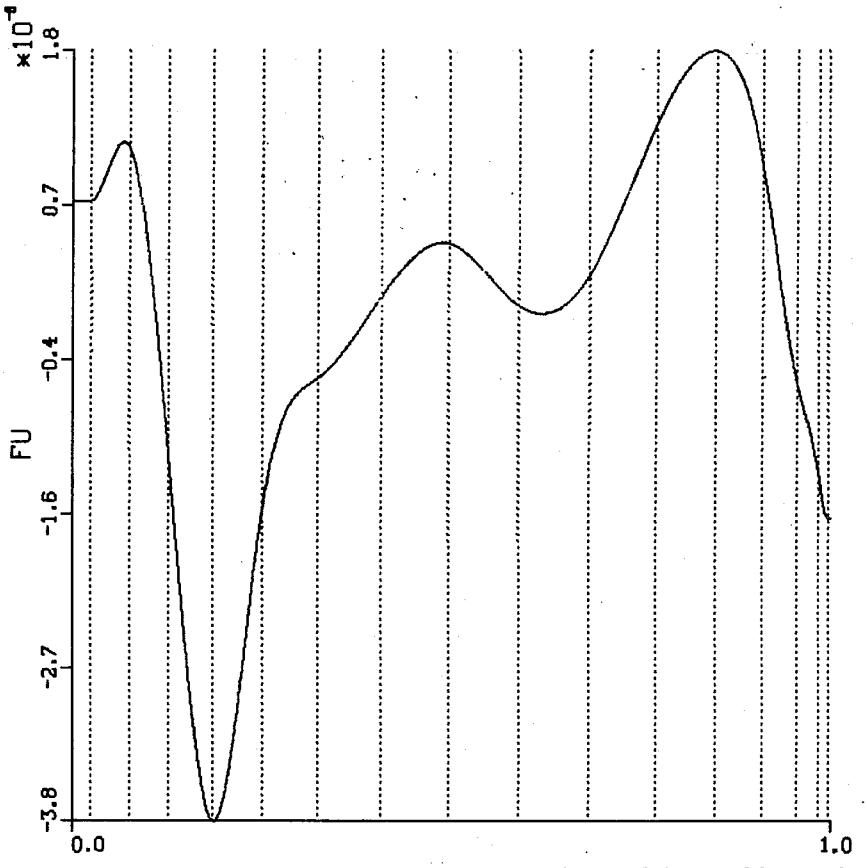

Fig. 2 Example of representation of a field by cubic splines in the vertical grid used with the ECMWF model.

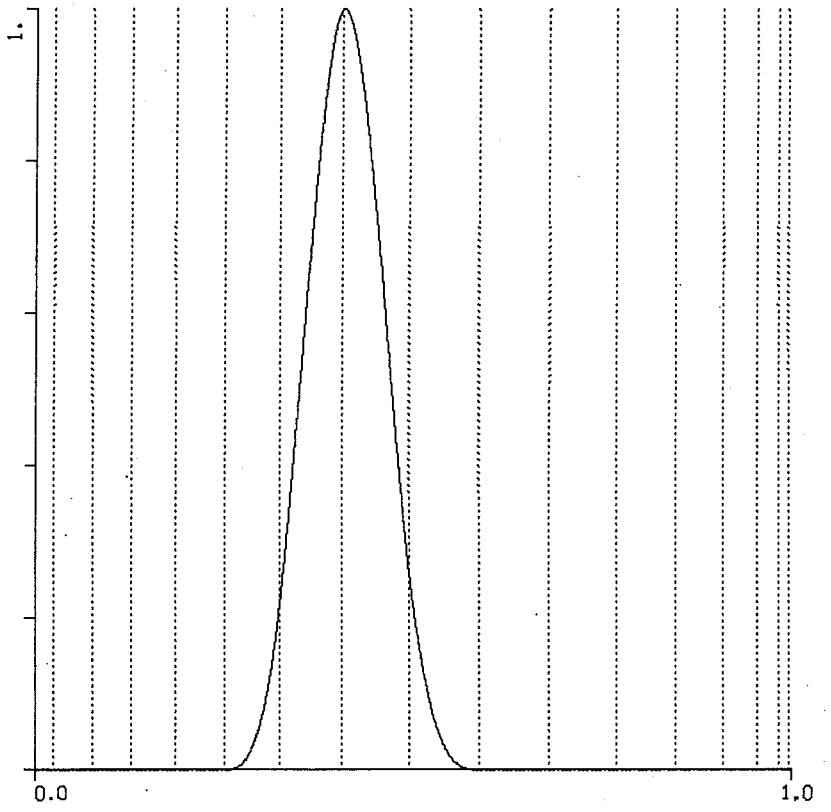

Fig. 3 Basis spline in the model grid.

nodepoints. For our purpose, it seems more appropriate to use the computation of first derivatives.

Let a field $\phi(\sigma)$ be given by its nodal values ϕ_ν, and define m_ν by

$$m_\nu = \left(\frac{\partial\phi}{\partial\sigma}\right)_\nu, \quad \nu \in \{1,\ldots,\text{NLEV}\} \tag{21}$$

For every interval $(\sigma_{\nu-1}, \sigma_\nu)$, $\nu \in \{2, \ldots, \text{NLEV}\}$, we have the following representation of ϕ and its derivatives:

$$\begin{aligned}\phi(\sigma) = {} & m_{\nu-1}\frac{(\sigma_\nu-\sigma)^2\,(\sigma-\sigma_{\nu-1})}{\Delta_\nu^2} \\ & - m_\nu \frac{(\sigma-\sigma_{\nu-1})^2\,(\sigma_\nu-\sigma)}{\Delta_\nu^2} \\ & + \phi_{\nu-1}\frac{(\sigma_\nu-\sigma)^2\,(2(\sigma-\sigma_{\nu-1})+\Delta_\nu)}{\Delta_\nu^3} \\ & + \phi_\nu \frac{(\sigma-\sigma_{\nu-1})^2\,(2(\sigma_\nu-\sigma)+\Delta_\nu)}{\Delta_\nu^3}\end{aligned} \tag{22}$$

$$\phi_\sigma(\sigma) = m_{\nu-1}\frac{(\sigma_\nu-\sigma)\,(2\sigma_{\nu-1}+\sigma_\nu-3\sigma)}{\Delta_\nu^2} \tag{23}$$

$$\begin{aligned} & -m_\nu \frac{(\sigma-\sigma_{\nu-1})\,(2\sigma_\nu+\sigma_{\nu-1}-3\sigma)}{\Delta_\nu^2} \\ & +6\frac{\phi_\nu-\phi_{\nu-1}}{\Delta_\nu^3}(\sigma_\nu-\sigma)\,(\sigma-\sigma_{\nu-1})\end{aligned} \tag{24}$$

$$\phi_{\sigma\sigma}(\sigma) = -2m_{\nu-1}\frac{2\sigma_\nu+\sigma_{\nu-1}-3\sigma}{\Delta_\nu^2} \tag{25}$$

$$- 2m_\nu \frac{2\sigma_{\nu-1}+\sigma_\nu-3\sigma}{\Delta_\nu^2} + 6\frac{\phi_\nu-\phi_{\nu-1}}{\Delta_\nu^3}(\sigma_\nu+\sigma_{\nu-1}-2\sigma)$$

where $\Delta_\nu = \sigma_\nu - \sigma_{\nu-1}$. For $\nu=1$ and $\nu=\text{NLEV}$ we have to specify two boundary conditions derived from the continuity of the first derivative. As pointed out above, we do not make a requirement concerning $\phi_{\sigma\sigma}$ at these nodepoints. The spline boundary conditions to be imposed will depend on the boundary treatment chosen for the linear part of the splines in the intervals $(0,\sigma_1)$ and $(\sigma_{\text{NLEV}}, 1)$.

In order to describe the cubic spline method for a rather general boundary treatment, we formulate the different boundary options by introducing field-values at $\sigma=0$ and $\sigma=1$, called ϕ_0 and ϕ_{NLEV+1}. For example, the temperature field treated by boundary B2 from Burridge et al. (1985) is given by

$$T_0 = T_1 \ , \ T_{NLEV+1} = T_{NLEV}$$

For ease of notation, we also introduce

$$\sigma_0=0, \ \sigma_{NLEV+1}=1 \tag{26}$$

Then the cubic spline boundary conditions are

$$m_1 = \frac{\phi_1-\phi_0}{\sigma_1-\sigma_0} = \frac{C_1}{2}$$

$$m_{NLEV} = \frac{\phi_{NLEV+1}-\phi_{NLEV}}{\sigma_{NLEV+1}-\sigma_{NLEV}} = \frac{C_{NLEV}}{2} \tag{27}$$

By (22) and (24), ϕ and ϕ_σ are continuous. The continuity of $\phi_{\sigma\sigma}$ will determine the m_ν for $\nu \in \{2,\ldots,NLEV-1\}$. From (25) we derive

$$\lambda_\nu m_{\nu-1}+2m_\nu+\mu_\nu m_{\nu+1}=C \tag{28}$$

with $\lambda_\nu = \dfrac{\Delta_{\nu+1}}{\Delta_\nu+\Delta_{\nu+1}} \qquad \mu_\nu=1-\lambda_\nu$

$$C_\nu=3\lambda_\nu \frac{\phi_\nu-\phi_{\nu-1}}{\Delta_\nu} +3\mu_\nu \frac{\phi_{\nu+1}-\phi_\nu}{\Delta_{\nu+1}} \tag{29}$$

Combining (27) and (28) we obtain the following set of equations for $m_1,\ldots,m_{NLEV}$

$$\begin{bmatrix} 2 & 0 & 0 & 0 & \cdots & & \\ \lambda_2 & 2 & \mu_2 & 0 & \cdots & & \\ 0 & \lambda_3 & 2 & \mu_3 & \cdots & & \\ & & \vdots & & \vdots & \vdots & \\ & & \cdots & \lambda_{NLEV-1} & 2 & \mu_{NLEV-1} \\ & & \cdots & 0 & 0 & 2 \end{bmatrix} \begin{bmatrix} m_1 \\ m_2 \\ m_3 \\ \vdots \\ m_{NLEV-1} \\ m_{NLEV} \end{bmatrix} = \begin{bmatrix} C_1 \\ C_2 \\ C_3 \\ \vdots \\ C_{NLEV-1} \\ C_{NLEV} \end{bmatrix} \tag{30}$$

(b) Minimum overlap spline basis

A spline basis e_{B_ν} of minimum overlap will probably be used only on the left-hand sides of the equations. Normally the representation as gridpoint values will be more convenient. Therefore only the transformations from b-spline to grid-representation need to be done. Away from the boundary, e_{B_ν} will be different from zero at three nodepoints. Therefore the amplitudes of this representation will not be gridpoint values of the fields. The basis spline will have the support of 4 grid intervals, so that the mass matrix of the FE-scheme will have 3 side-diagonals. A basis spline function is shown in Fig. 3.

The interpolation formula given in the previous section provides the polynomial representation of the spline, provided that node values and values of the derivatives at nodepoints are given. Scalar products and field values at intermediate points can be formed using this polynomial representation. Therefore we must determine the gridpoint values and node derivatives of the b-splines.

We associate a b-spline with every model level and distinguish between three kinds of b-spline definition according to their vicinity to the boundary $\nu=1$ and $\nu=NLEV$. Here the definition of the boundary splines only for the case of the upper boundary $\nu=1$ will be given.

The definition of the splines is given by the following conditions:

for $\mu \neq 1, 2, NLEV, NLEV-1$

$$\chi^{\nu}(\sigma_{\nu\pm2}) = 0 \qquad \text{(a)}$$
$$\chi^{\nu}(\sigma_{\nu}) = 1 \qquad \text{(b)} \qquad (31)$$
$$\chi^{\nu}_{\sigma}(\sigma_{\nu\pm2}) = 0 \qquad \text{(c)}$$
$$\chi^{\nu}_{\sigma\sigma}(\sigma_{\nu\pm2}) = 0 \qquad \text{(d)}$$

The spline for $\mu = 2$ is defined by:

$$\chi^{2}(\sigma_{2+2}) = 0 \qquad \text{(a)}$$
$$\chi^{2}(\sigma_{2}) = 1 \qquad \text{(b)}$$
$$\chi^{2}_{\sigma}(\sigma_{2+2}) = 0 \qquad \text{(c)} \qquad (32)$$
$$\chi^{2}_{\sigma\sigma}(\sigma_{2+2}) = 0 \qquad \text{(d)}$$
$$\chi^{2}_{\sigma}(\sigma_{1}) = \frac{\chi^{2}(\sigma_{1})}{\sigma_{1}} \qquad \text{(e)}$$
$$\chi^{2}_{\sigma\sigma}(\sigma_{1}) = 0 \qquad \text{(f)}$$

For $\mu = 1$ we have the definition:

$$\chi^{1}(\sigma_{1+2}) = 0 \qquad \text{(a)}$$
$$\chi^{1}(\sigma_{1}) = 1 \qquad \text{(b)}$$
$$\chi^{1}_{\sigma}(\sigma_{1+2}) = 0 \qquad \text{(c)} \qquad (33)$$
$$\chi^{1}_{\sigma}(\sigma_{1}) = \frac{1}{\sigma_{1}} \qquad \text{(d)}$$
$$\chi^{1}_{\sigma\sigma}(\sigma_{1+2}) = 0 \qquad \text{(e)}$$

According to Section 3.2(a) the spline is known if in (31) the conditions on $\chi^{\nu}_{\sigma\sigma}$ are expressed by computing the nodepoint-values of $\chi^{\nu\pm1}$. It is sufficient to describe this procedure for the spline not adjacent to the boundary, defined in (31).

This spline is composed of three auxiliary splines ${}^1\chi^\nu$, ${}^2\chi^\nu$, ${}^3\chi^\nu$ defined according to Section 3.2(a) by the conditions

$$ {}^2\chi^\nu(\sigma_{\nu\pm1}) = 0 \quad \text{and (31) a,b,c} \tag{34} $$

$$ {}^1\chi^\nu(\sigma_\nu) = {}^1\chi^\nu(\sigma_{\nu+1}) = 0 \tag{35} $$

$$ {}^1\chi^\nu(\sigma_{\nu-1}) = 1 \quad \text{and (31) a,c} $$

$$ {}^3\chi^\nu(\sigma_\nu) = {}^3\chi^\nu(\sigma_{\nu-1}) = 0 $$

$$ {}^3\chi^\nu(\sigma_{\nu+1}) = 1 \text{ and (31) a,c} \tag{36} $$

Let ${}^\zeta m_\nu^\nu$ be the nodal slopes belonging to the splines ${}^\zeta\chi^\nu$, as computed according to Section 3.2(a).

Let us form χ^ν as

$$ \chi^\nu(\sigma) = {}^2\chi^\nu(\sigma) + \alpha\ {}^1\chi^\nu(\sigma) + \beta\ {}^3\chi^\nu(\sigma) $$

From (31d, 24) we obtain two equations for α and β

$$ \alpha\ {}^1m_{\nu+1}^\nu + \beta\ {}^3m_{\nu+1}^\nu + {}^2m_{\nu+1}^\nu + \frac{{}^3\chi^3_{\nu+1}}{\Delta_{\nu+2}} = 0 $$

$$ -\alpha\ {}^1m_{\nu-1}^\nu - \beta\ {}^3m_{\nu-1}^\nu + {}^2m_{\nu-1}^\nu + \frac{{}^3\chi^3_{\nu-1}}{\Delta_{\nu-1}} = 0 \tag{37} $$

for $-\ {}^1m_{\nu+1}^\nu\ {}^3m_{\nu-1}^\nu + {}^3m_{\nu+1}^\nu\ {}^1m_{\nu-1}^\nu \neq 0$

(37) can be solved for α and β, which are the required nodepoint values.

(c) Transformations to intermediate bases

We will use two kinds of intermediate representations: the interpolation to a finer grid and the representation by Taylor coefficients. In both cases we will first have to compute the m_ν according to Section 3.2(a).

For the transformation to a finer grid, let $\breve{\sigma}_1, \ldots, \breve{\sigma}_T \in (\sigma_{\nu-1}, \sigma_\nu)$ be given. From (22) and (24) we get the transformation by using $\sigma = \breve{\sigma}_\zeta$.

For the computation of Taylor coefficients assume a point $\breve{\sigma} \varepsilon (\sigma_{\nu-1}, \sigma_\nu)$, about which the development is taken:

$$\phi(\sigma)=\phi_0+\phi_1(\sigma-\breve{\sigma})+\phi_2(\sigma-\breve{\sigma})^2+\phi_3(\sigma-\breve{\sigma})^3 \text{ for } \sigma \varepsilon (\sigma_{\nu-1},\sigma_\nu) \tag{38}$$

with $\phi_0=\phi(\breve{\sigma})$

$$\phi_1=\phi_\sigma(\breve{\sigma}) \tag{39}$$

$$\phi_2=\frac{1}{2}\phi_{\sigma\sigma}(\breve{\sigma})$$

$$\phi_3=\frac{1}{6}\phi_{\sigma\sigma\sigma}(\breve{\sigma})$$

We have

$$\phi_{\sigma\sigma\sigma}(\breve{\sigma}) = \frac{6\breve{\sigma}}{\Delta_\nu^2}(m_{\nu-1}+m_\nu) - \frac{12\breve{\sigma}}{\Delta_\nu^3}(\phi_\nu-\phi_{\nu-1}) \tag{40}$$

and the other derivatives of ϕ can be taken from (22)-(25).

3.3 Operation counts

As an illustration consider the representation of fields ϕ^1 and ϕ^2 by the b-splines of Section 3.2(b).

$$\phi^\zeta(\sigma)=\sum_\nu \alpha_\nu^\zeta \chi^\nu(\sigma) \qquad \zeta\varepsilon\{1,2\} \tag{41}$$

A b-spline χ^μ overlaps 7 other b-splines. Therefore by programming the scalar product of χ^μ with the product of ϕ^1 and ϕ^2 in the straightforward way

$$(\chi^\mu,\phi^1\phi^2) = \sum_{\nu_1\varepsilon M}\sum_{\nu_2\varepsilon M} W^{\nu_1,\nu_2}\,\phi^1_{\nu_1}\cdot\phi^2_{\nu_2} \tag{42}$$

with $W^{\nu_1,\nu_2} = (\chi^{\nu_1},\chi^{\nu_2})$

and M being the set of indices ν whose χ^ν overlap with χ^μ, we obtain 2x49 multiplications for an operation whose gridpoint equivalent cost is one multiplication.

This example shows that even for a research model it is necessary to consider the organisation of the model in order not to incur an excessive computational cost.

Basically, the discretization given in (42) is the same as used in Burridge et al. (1985).

For the linear FE-scheme, the operation count is 18; by algebraic manipulation, using the fact that many of the weights are equal, this is reduced to 11.

In this study, the intention is not to go into detail concerning optimization. Therefore we will consider only the discretization of the product of two different fields ϕ^1 and ϕ^2. This term is probably not responsible for the advantages of the FE-scheme; energy transformation terms and the vertical advection terms are the more likely cause of these. However, as discretized in the ECMWF linear FE-models, it is responsible for a lot of the computational expense of the schemes since many products of fields have to be taken.

For simplicity we count only multiplications and consider the number of intervals $(\sigma_{\nu-1}, \sigma_\nu)$ as equal to the number of model levels, ignoring overheads associated with boundary elements. We also do not consider the computational overheads incurred in transforming the fields; for example the transformation to a finer grid for the collocation method, and the Gaussian inversion leading from scalar products to the amplitude space.

We consider only computations using grid interval associated qualities, meaning that a set of numbers is computed associated with each $(\sigma_{\nu-1}, \sigma_\nu)$ which will be used for the computation of several amplitudes. The method indicated in (42) will not be considered. For comparison, we consider also the linear elements.

For the quadratic spline, half values may appear as operation counts since there are two kinds of amplitudes for which the average has to be taken.

For the collocation method, we use Lobatto's integration, which is the equivalent of a Gaussian integration with the additional requirement that the end-points of the integration interval are nodepoints for the integration.

Let $\tilde{\sigma}_\nu$, $\nu \in \{0,..,n\}$, $\tilde{\sigma}_0=\sigma_{\nu-1}$, $\tilde{\sigma}_n=\sigma_\nu$ be the collocation points associated with the interval $(\sigma_{\nu-1},\sigma_\nu)$.

The integration formula is

$$\int_{\sigma_{\nu-1}}^{\sigma_\nu} f(\sigma)d\sigma=\sum_{\xi=0}^{n} f(\tilde{\sigma}_\xi)W_\xi \tag{43}$$

Let d be the maximum degree of the polynomials which are to be computed exactly. We then obtain the condition

$$n > \frac{d}{2} +1 \tag{44}$$

where n is the number of collocation points necessary per grid point.

The resulting number of collocation points is listed in Table 1.

Method	1st order FE	2nd order FE	cubic spline FE
Number of of collocation points	3	5	6

Table 1 Number of collocation points necessary for different methods

The interval basis is assumed to be

$$f(\sigma)=\sum_{\nu=0}^{\sigma} C_\nu(\sigma-\sigma_0)^\nu \quad \text{for } \sigma \in (\sigma_{\nu-1},\sigma_\nu) \tag{44}$$

with $\sigma=2$ for second order and $\sigma=3$ for cubic spline elements.

The transformation to zero-node splines is described in Section 3.1(e).

For example consider the second order FE-method. The spline P to be subtracted for the product $f^1(\sigma)\, f^2(\sigma)$ is, according to (8) given by

$$P_\nu = f^1_\nu f^2_\nu \quad \text{for } \nu \in F$$

and

$$P_{\sigma\sigma_\nu} = \bar{f}^1_\nu f^2_{\sigma\sigma_\nu} + f^1_{\sigma\sigma_\nu}\bar{f}^2_\nu + w_\nu(f^1_{\nu+1}-f^2_{\nu-1})(f^2_{\nu+1}-f^2_{\nu-1}) \quad \text{for } \nu \in H \tag{45}$$

with $\bar{f}^\rho = \frac{1}{2}(f^\rho_{\nu-1}+f^\rho_{\nu+1})$, $\bar{\sigma}=\frac{1}{2}(\sigma_\nu+\sigma_{\nu+1})$ and w_ν being a weight factor.

To derive (45), represent f^ρ for $\sigma \in (\sigma_{\nu-1},\sigma_{\nu+1})$ in the form

$$f^\rho = \bar{f}^\rho + \frac{f_{\nu+1}-f_{\nu-1}}{\sigma_{\nu+1}-\sigma_{\nu-1}}(\sigma-\bar{\sigma}) + f^\rho_{\sigma\sigma_\nu} h_\nu(\sigma)$$

From (45) we need 1+4 multiplications. For every interval $(\sigma_{\nu-1}, \sigma_{\nu+1})$, $\nu \in H$, we have to compute three linearly independent amplitudes, $f^1_{\sigma\sigma_\nu} f^2_{\sigma\sigma_\nu}$, $f^1_{\sigma\sigma_\nu} (f^2_{\nu+1}-f^2_{\nu-1})$, $(f^1_{\nu+1}-f^1_{\nu-1})f^2_{\sigma\sigma\sigma_\nu}$ needing three multiplications. The three amplitudes associated with an interval $(\sigma_{\nu-1}, \sigma_{\nu+1})$ have to be multiplied with weights in order to get the scalar product with the basis functions. Since the basis function e_ν of (8) overlaps two intervals, and h_ν overlaps one interval, we need 6 and 3 multiplications for this.

A factor $\frac{1}{2}$ has to be applied because for second order elements one grid interval $(\sigma_{\nu-1}, \sigma_{\nu+1})$ supports two amplitudes. So we arrive at an operation count of 8.5 multiplications.

The other computation methods have also an expense associated with each interval and another one associated with the formation of the scalar products. In all cases, the second part of the computation is more expensive than the first because the basis functions overlap many intervals. This is mainly the reason for the relative economy of the second order FE-method and the high expense of the cubic spline method.

Table 2 gives the operation count for the methods mentioned.

The higher order FE-methods proposed can be considered as further developments of the linear FE-method in Burridge et al. (1985). The computational costs of the implementation of this method in the spectral model was 5 to 6%.

When choosing a method of computation, it should be noted that the methods of interval-bases and transformation to σ-node splines can be applied also to the product involving the ω-term and the grad ϕ term. The operation count will then change slightly compared with Table 2. The direct application of the

collocation method is not possible for these terms. Therefore it will be necessary to use interval bases for this term or to do algebraic transformations on these terms to separate a part which can be computed by collocation.

	as implemented with 1st order ECMWF-FE method	collocation method	interval bases	transformation to 0-node spline
grid model	1	-	-	-
1st order FE	11	3+2x3 = 9	4+2x3 = 10	1+1+2 = 4
2nd order FE	-	$\frac{1}{2}$.5+$\frac{1}{2}$(2x5+5) = 10	$\frac{1}{2}$.9+$\frac{1}{2}$(2x5+5) = 12	$\frac{1}{2}$(1+4+3)+$\frac{1}{2}$(6+3) = 8.5
Cubic spline FE	-	6+4x6 = 30	16+4x7 = 44	-

Table 2 Operation counts for different methods

Table 2 is intended to give only a rough estimate of the expense of the FE-methods. We may draw the following conclusions.

a) For first and second order finite elements, the transformation to σ-node splines seems most appropriate. For the cubic splines, the collocation method will be the most economic.

b) The cost of the second order elements is not excessively above that of the first order elements. It should be possible to implement the second order elements within the time used by the linear FE methods presently implemented at ECMWF.

c) The cubic spline FE method is quite expensive, but its expense remains reasonable for a research version of the model. If instead of using the full Galerkin procedure one introduces simplifications like the employment of fewer collocation points, there is some scope for making it computationally less expensive.

3.4 Gaussian inversion

For second order splines we need to solve only equations involving a one sided diagonal matrix. These are treated in the same way as for the linear elements. For the cubic spline-elements, we need the Gaussian inversion procedure with three side diagonal matrices, which will now be discussed.

Let the matrix equation be given as

$$\begin{bmatrix} A_{11}, A_{12}, A_{13}, A_{14}, 0, 0, \ldots\ldots\ldots \\ A_{21}, A_{22}, A_{23}, A_{24}, A_{25}, 0, \ldots\ldots\ldots \\ A_{31}, A_{32}, A_{33}, A_{34}, A_{35}, A_{36}, \ldots\ldots\ldots \\ A_{41}, A_{42}, A_{43}, A_{44}, A_{45}, A_{46}, \\ 0, A_{52}, A_{53}, A_{54}, A_{55}, A_{57}, \\ 0, 0, A_{63}, A_{64}, A_{65}, A_{66}, \\ \end{bmatrix} \begin{bmatrix} X_1 \\ X_2 \\ X_3 \\ X_4 \\ X_5 \\ X_6 \\ \vdots \end{bmatrix} = \begin{bmatrix} C_1 \\ C_2 \\ C_3 \\ C_4 \\ C_5 \\ C_6 \\ \vdots \end{bmatrix} \qquad (46)$$

The side diagonals are $A_{\nu,\nu\pm\mu} \neq 0$ for $\mu \in \{0,1,2,3\}$

The solution is achieved by the following set of substitutions:

for $\mu = 1, \ldots, NLEV-1$ successively

$$A_{\kappa,\mu+\nu} \Longrightarrow A_{\kappa,\mu+\nu} - \frac{A_{\kappa,\mu}}{A_{\mu,\mu}} A_{\mu,\mu+\nu}$$

$$C_\kappa \Longrightarrow C_\kappa - \frac{A_{\kappa,\mu}}{A_{\mu,\mu}} C_\mu \qquad (47)$$

The solution is then obtained by

$$X_{NLEV} = \frac{C_{NLEV}}{A_{NLEV,NLEV}}$$

$$X_\kappa = \frac{C_\kappa - \sum_{\nu=\kappa+1}^{\alpha} A_{\kappa,\nu} X_{\kappa,\nu}}{A_{\kappa,\kappa}} \qquad (48)$$

$\alpha = \min(\kappa+3, NLEV)$

4. NUMERICAL EXPERIMENTS

The second order elements were implemented using the transformation to zero-node splines and the interval basis method. The cubic spline elements were implemented by the collocation method. According to Section 3.3 these are the most efficient approaches. Since the top model interval uses linear interpolation of the fields, the formulations of boundary elements given in Section 2.4 of Burridge et al. (1985) can immediately be applied. The quadratic splines were formulated using boundary treatment B4 of Burridge et al. (1985). The cubic splines use a simplified treatment of the boundary obtained by extending the Galerkin integrals from σ_1 to 1 instead of from 0 to 1. According to calculations with horizontal resolution T21 and linear elements, this is not a very good formulation and the results are likely to suffer from it. However, a more sophisticated boundary formulation with the third order scheme was left until a formulation of the scheme in the hybrid coordinate used operationally at ECMWF is available.

4.1 Data assimilation

Experiments were performed from 12Z, 20.1.85 using a σ-coordinate version of the ECMWF operational model and the cubic spline finite element model to produce the first guess. The σ_ν values can be seen in Fig. 2. The first guess error was evaluated directly against measurements. The cubic spline finite element model reduced this error already after the first 6 hour cycle. Figs. 4 and 5 show the first guess errors after 12 hours of assimilation for the northern and southern hemispheres. The assimilation cycle was continued for 3 days. The reduction of error by the cubic spline method, as shown in Figs. 4 and 5, was typical of the whole cycle.

Figs. 6 and 7 show the comparison of first guess errors for first and third order elements. The treatment of the first order elements at the top of the atmosphere was simplified in the same way as described for the third order elements. In the upper part of the atmosphere, the third order elements give better results than the first order ones.

Forecasts were run from these analyses with the cubic spline model, and the σ-coordinate version of the operational model. After 3-5 days, the FE-model became unstable due to small scale features being present in the top level of the analysis. The investigation of this problem was postponed until the development of a hybrid-coordinate FE-scheme. Up to day 3.5 the anomaly correlations are shown in Fig. 8. There is some advantage of the FE-scheme for wavenumbers 10-20 and to a lesser extent for wavenumbers 4-9. However, with the total scores being very little improved, the difference in the forecasts is not of great relevance up to day 3.5.

4.2 10 day forecasts

(a) Objective verification

Ten day integrations were performed for two sets of 6 initial dates, given in Table 3. Set 1 consists of the same dates used by Burridge et al. (1985) for test runs. Model runs were performed with quadratic elements for both sets (12 cases) whilst the cubic spline scheme was tested for Set 2 (6 cases). For a subset of Set 2 (cases 2,3,6) computations were carried out with linear elements, using the same simplifications at the top boundary as employed with the cubic spline elements. Set 2 results in very good forecasts, with the height-anomaly correlation staying above 60% for the whole 10 day period in most of the cases.

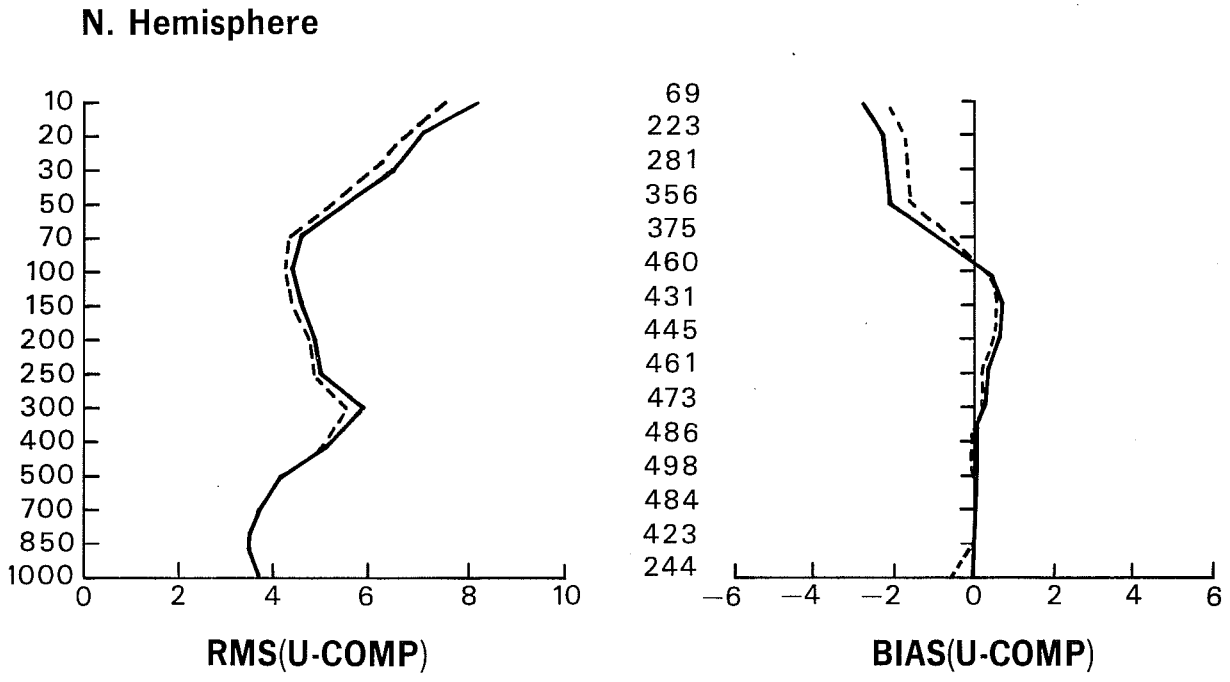

Fig. 4 First guess rms error and bias in the northern hemisphere for the u-velocity component after 12 hours of assimilation. Solid = control, dashed = cubic spline finite element model.

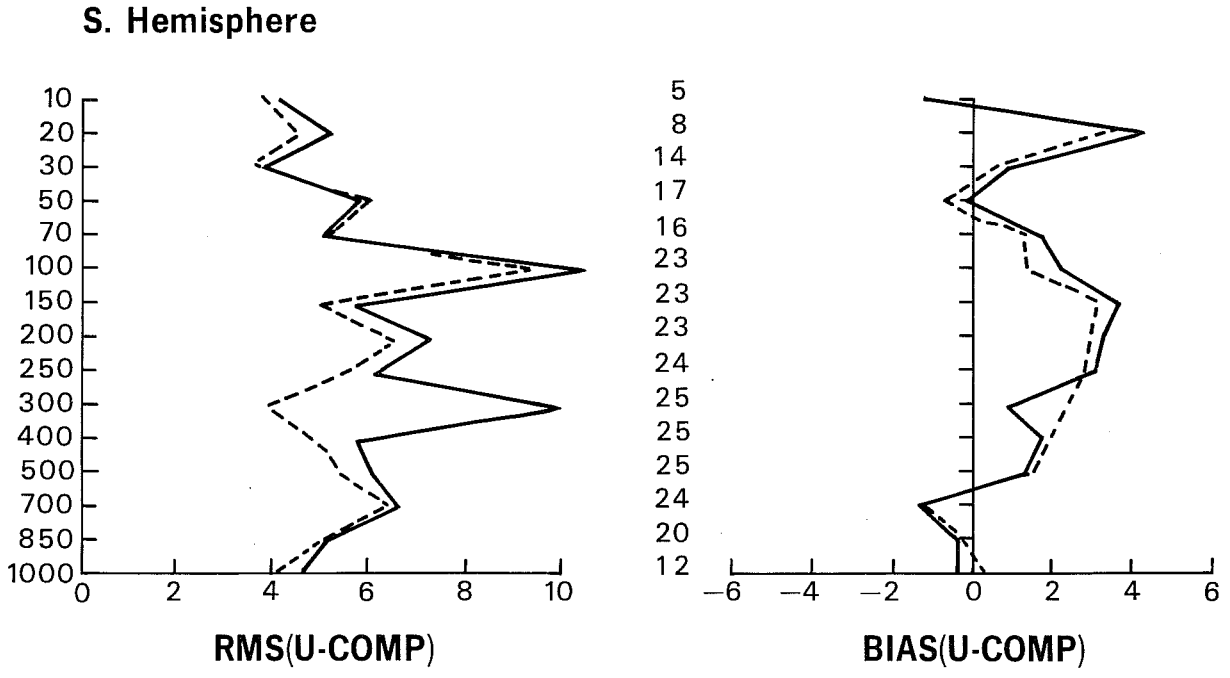

Fig. 5 As Fig. 4, for the southern hemisphere

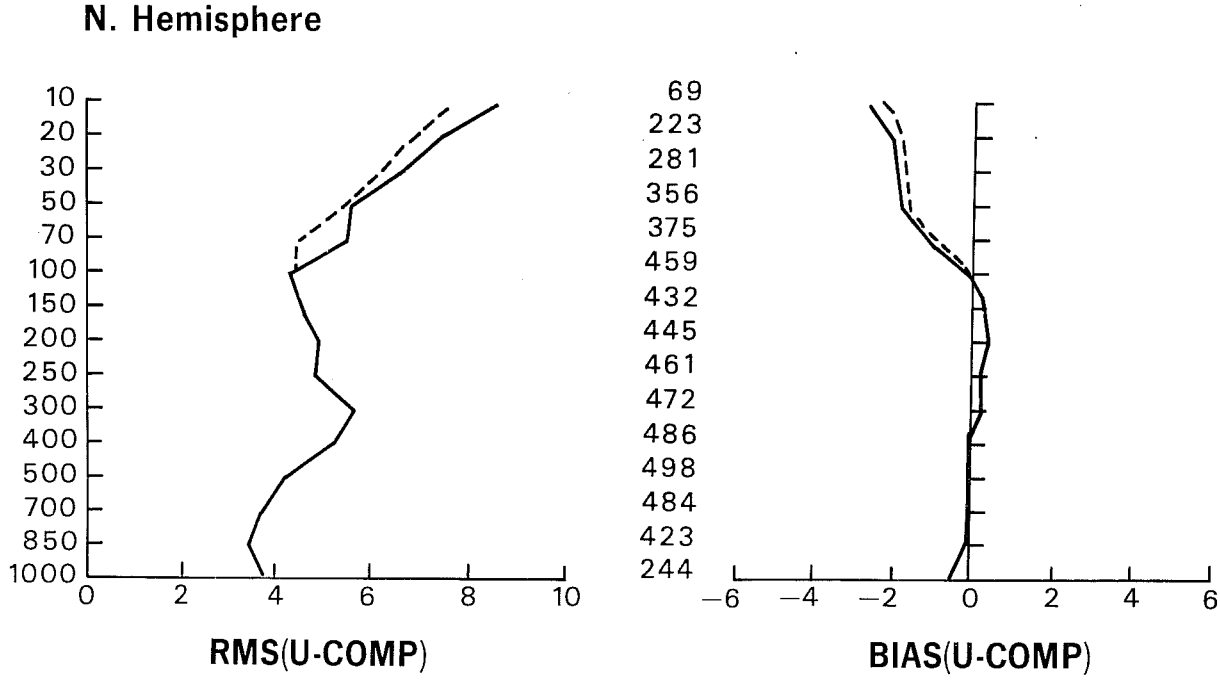

Fig. 6 First guess rms error and bias in the northern hemisphere for the u-velocity component after 12 hours of assimilation. Solid = linear finite elements, dashed = cubic spline finite elements.

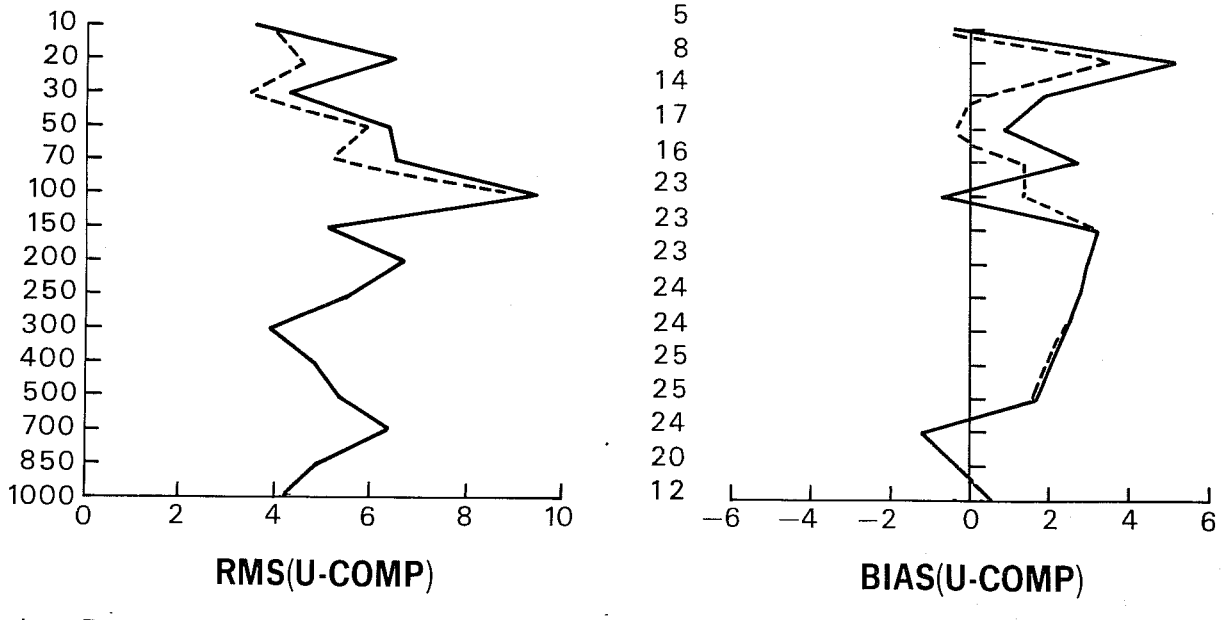

Fig. 7 As Fig. 6, for the southern hemisphere

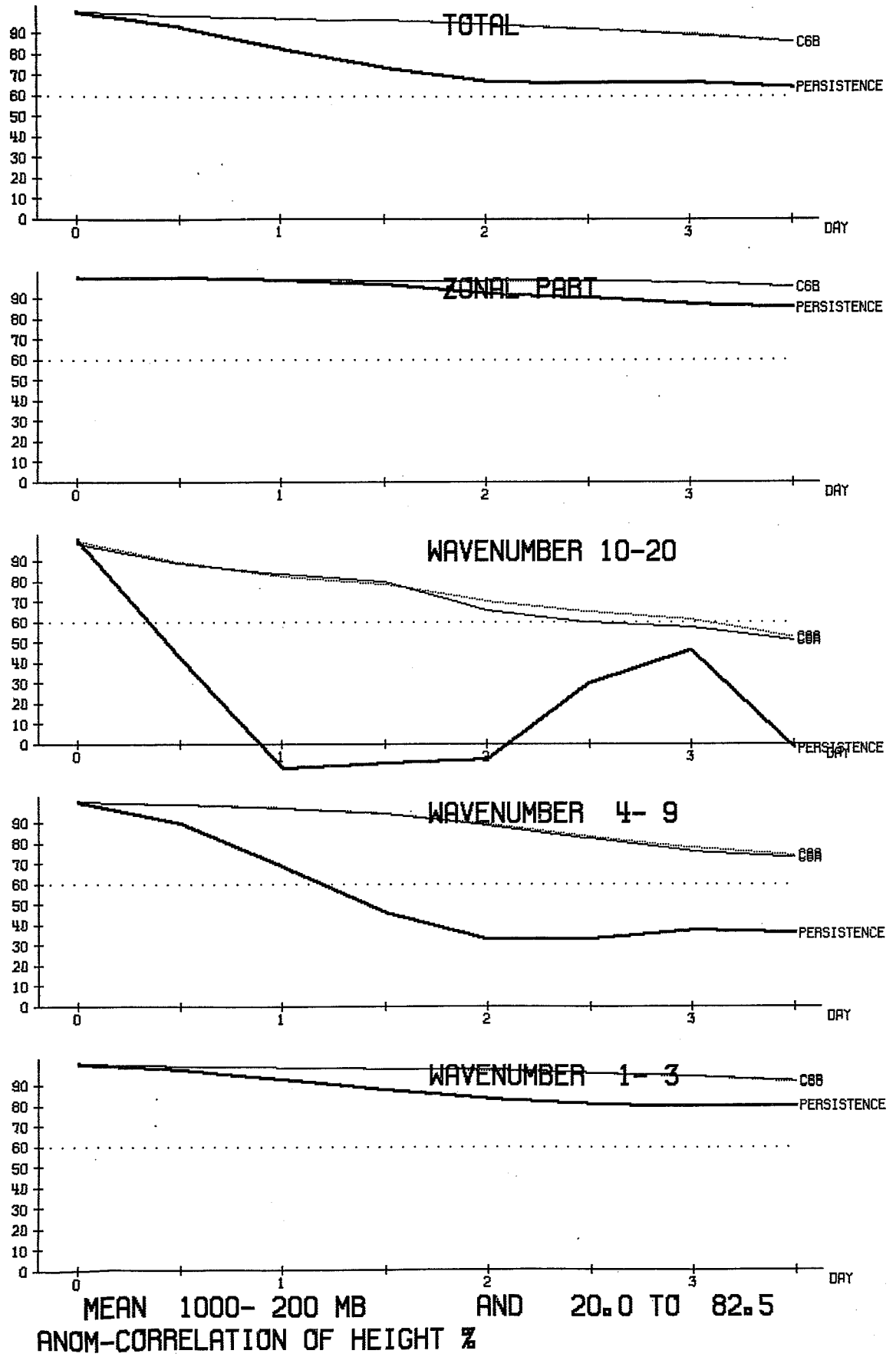

Fig. 8 Anomaly correlations for run from data assimilation cycle. Solid = control, dotted = cubic spline elements, think solid line persistence forecast.

Case No.	Set 1	Set 2
1	16.8.83	1.1.85
2	25.12.83	10.1.85
3	1.1.84	20.1.85
4	10.1.84	30.1.85
5	23.8.83	10.1.84
6	7.4.83	20.1.84

Table 3 The initial date for 10-day test integrations

The experiments were compared for a range of days where nearly all correlations remained above 40%; days 5 to 8 were used for Set 1. Since Set 2 was a set of extremely good forecasts, days 5 to 10 were used with this set. The model used for the control was a σ-coordinate version of the ECMWF operational model. Fig. 9 shows the scatter diagram comparing the control runs with the corresponding experiments using second order finite elements for days 5,6,7,8; total anomaly correlations of height, averaged for 1000 to 200 mb, are compared. For Set 2, the corresponding diagram is given in Fig. 10, whilst Fig. 11 gives the results for the cubic spline elements. It appears that all methods produce an almost systematic improvement compared with the control runs, with nearly all points being on one side of the diagonal. There is no systematic relationship between second and third order or second and first order elements; different methods give the best improvement on different dates. This may partly be due to the fact that the boundary treatment for the second order elements is different from that of the other finite element methods: the second order elements use the B4-boundary of Burridge et al. (1985), first order element runs are available for B1 and B2 boundaries, and the cubic spline method uses a simplified boundary treatment.

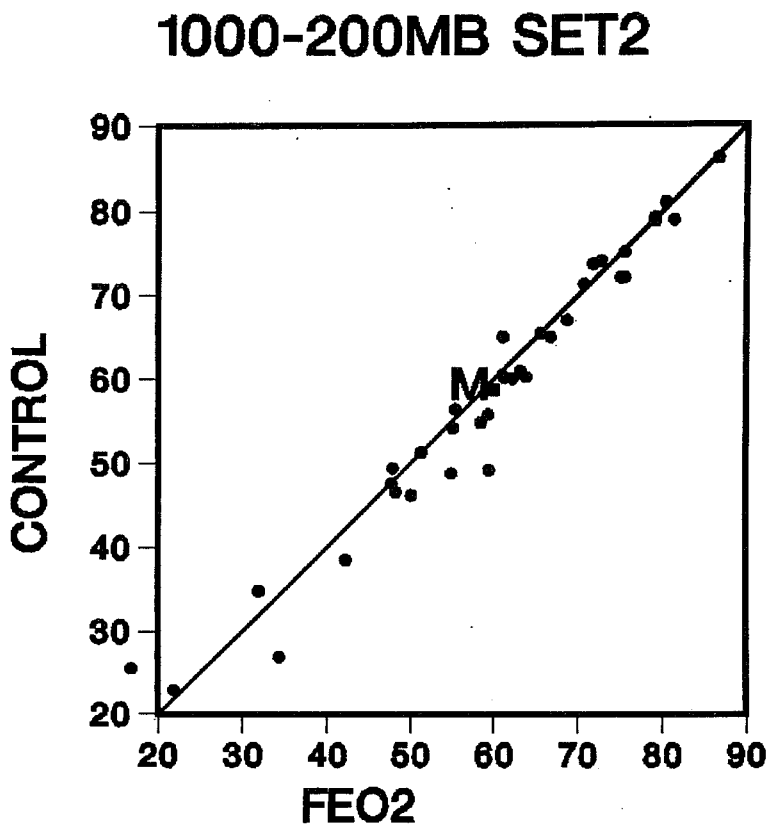

Fig. 9 Total anomaly correlations of height, 1000-200 mb, scatter diagram comparing control run and second order finite elements for set 1, days 5,6,7,8.

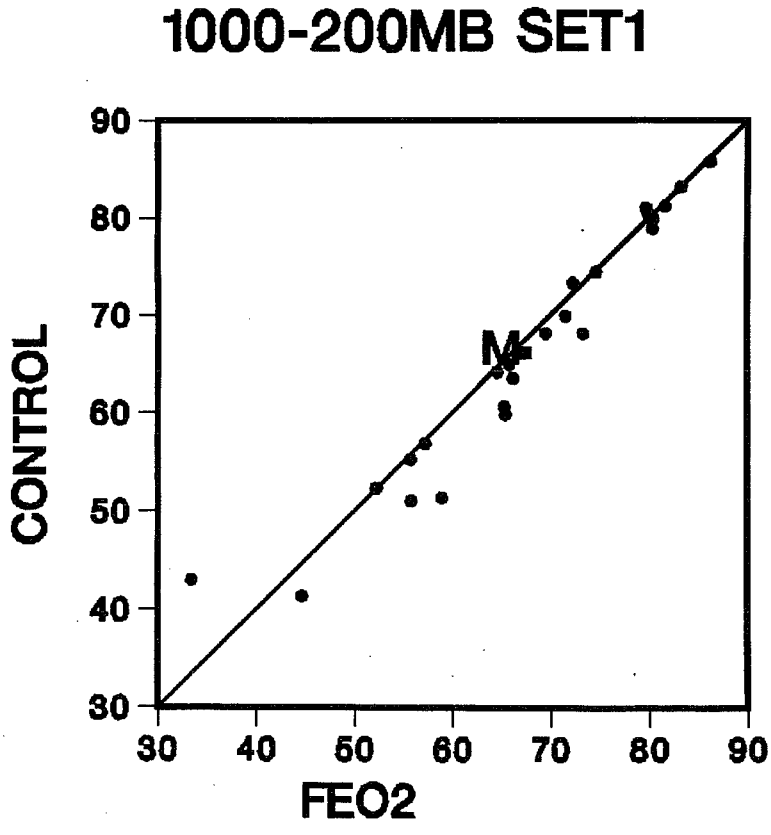

Fig. 10 As Fig. 9, for set 2, days 5,6,7,8,9,10.

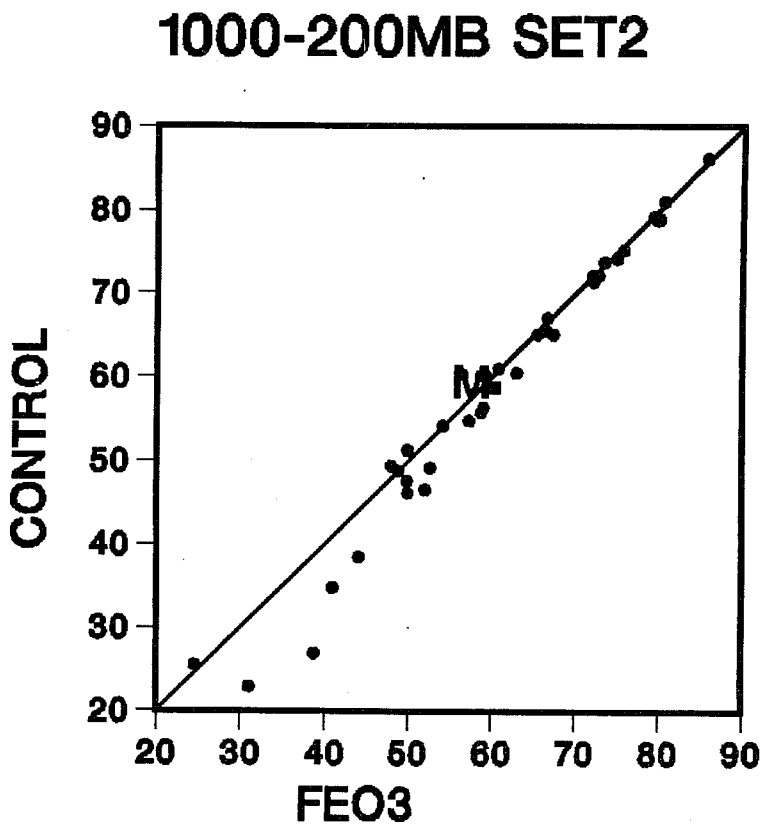

Fig. 11 As Fig. 9, for cubic spline elements, set 2, days 5,6,7,8,9,10.

Furthermore, the linear analysis given in Steppeler (1975) indicates that quadratic splines improve the accuracy of difference models only for wavelength greater than $4\Delta x$. There may well be a range of wavenumbers smaller than $4\Delta x$ for which linear elements have a better accuracy. For the investigation of a possible difference in performance of high and low order elements a comparison of order 1 and order 3 elements seems therefore most appropriate.

The differences between finite element and control runs are smaller than those encountered between the spectral method and a second order finite differencing in the horizontal as described in Girard and Jarraud (1982). Typically, the finite element scheme encounters the same differences at day 7 which the spectral method had after 4 days. However, the present results indicate a rather systematic increase of forecast skill.

For the finite element schemes, the average increase of the height anomaly correlation of the different forecast days are given in Fig. 12. The increase of forecast skill for both methods reaches the same order of magnitude as for the comparison of spectral and grid point methods (Girard and Jarraud, 1982). However, some sampling error may be present since the present study uses a rather limited set of cases, with only 2 summer cases being present.

Fig. 13 gives the standard deviation of temperature for the ensemble average of Set 2. Again a small improvement of the cubic spline elements over the control run is apparent, however comparison of second and first order elements does not give a clear indication of which one of them is best. The detection of small differences in forecast skill is difficult because they do not improve systematically. Compared with the control run, the cases which show the best improvement are different for linear and quadratic elements.

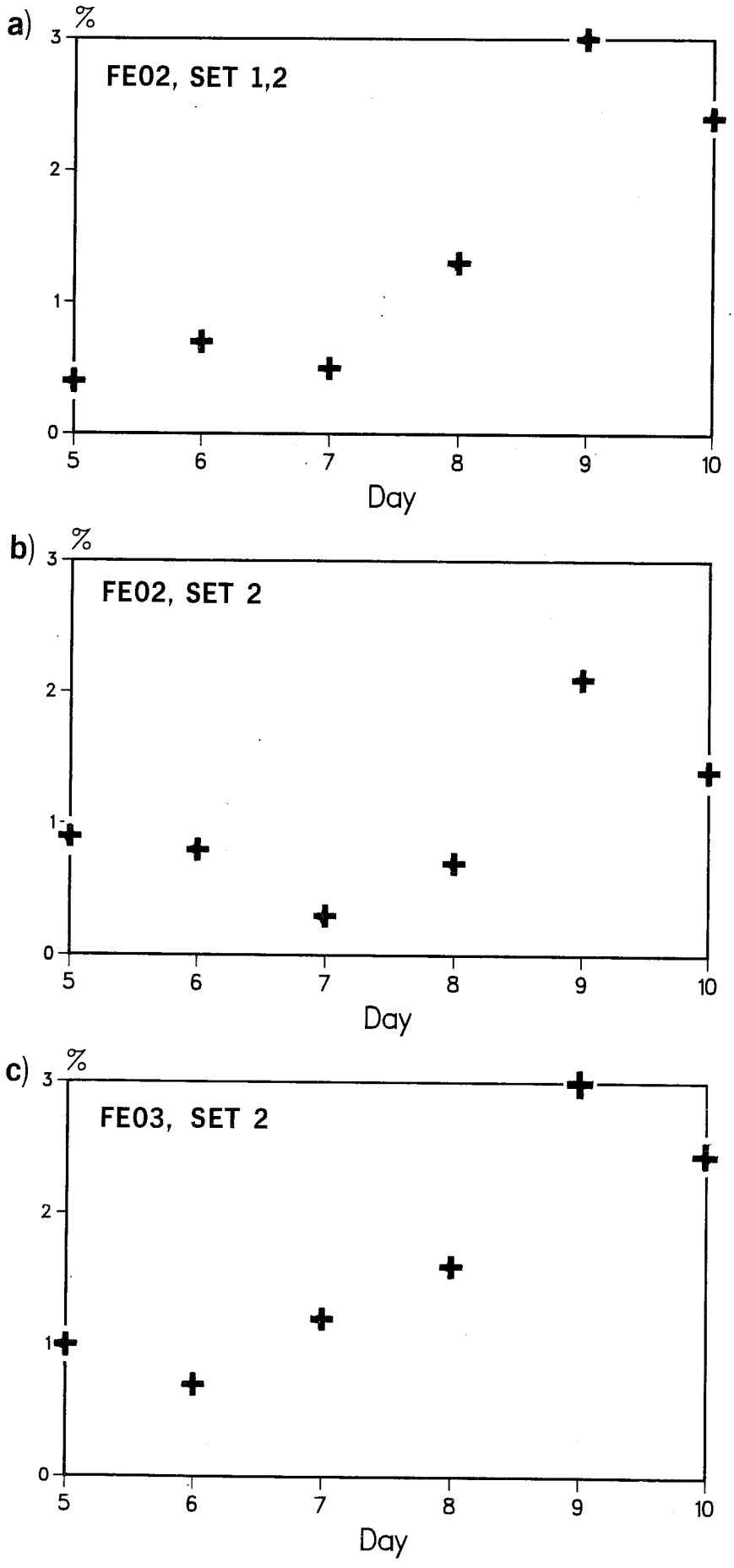

Fig. 12 Average increase of anomaly correlation of height, 1000-200 mb (a), second order elements, combined sets 1,2; (b) second order elements, set 2: (c) cubic spline elements, set 2.

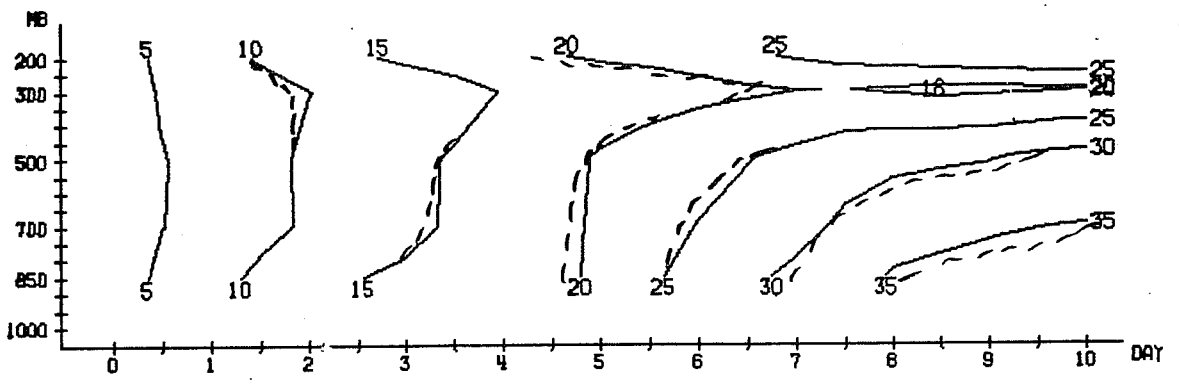

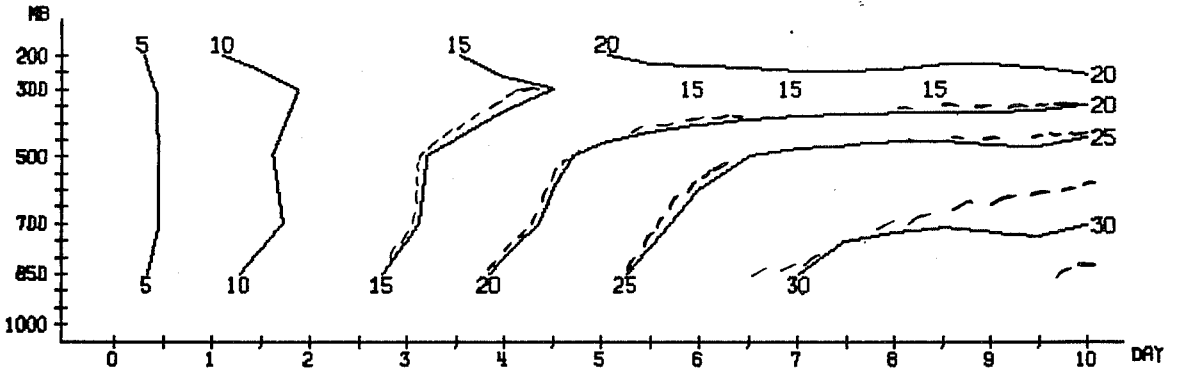

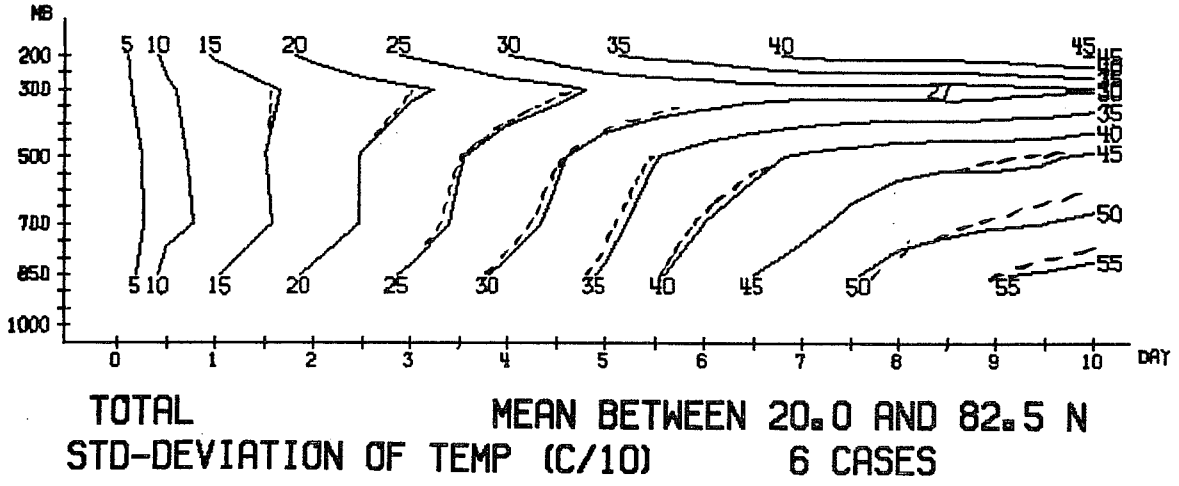

Fig. 13 Ensemble average standard deviation of temperature, set 2
solid = control, dashed = cubic spline finite elements.

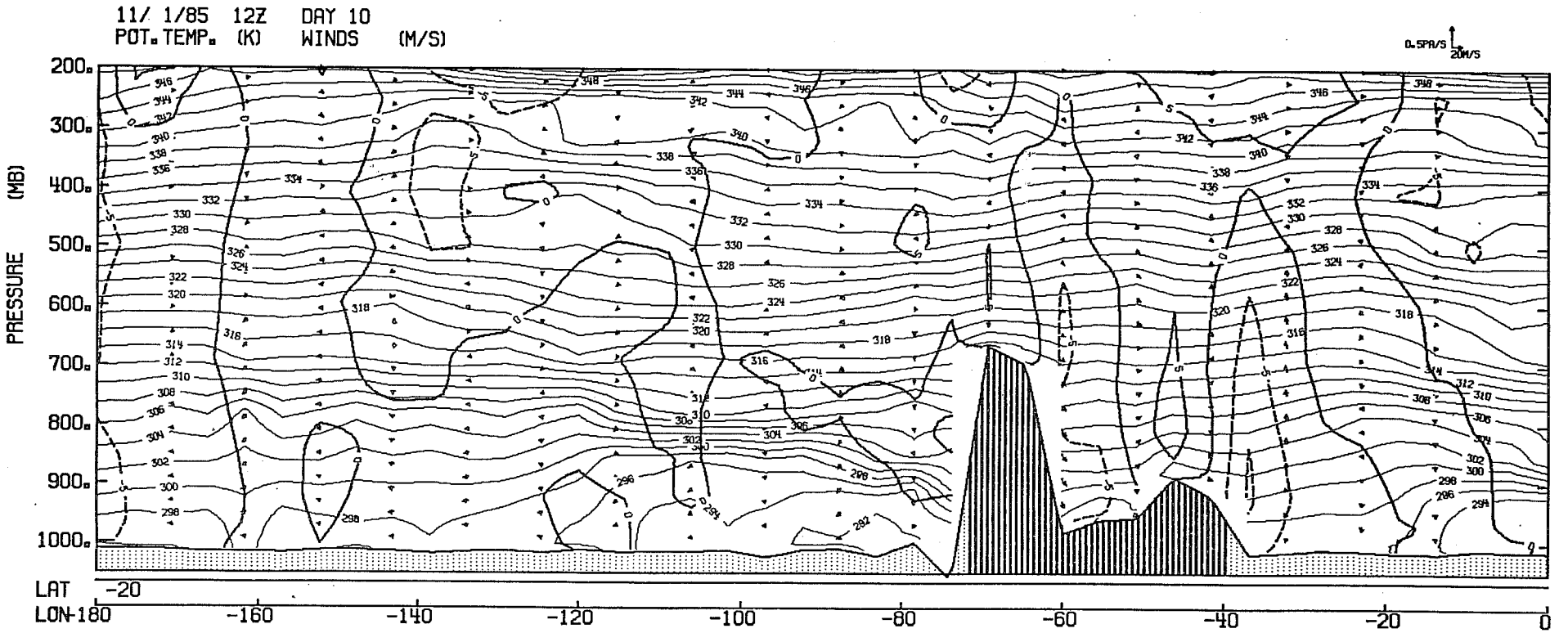

Fig. 14 Vertical cross section, day 10, for cubic spline finite elements, initial date 1.1.85.

Computational modes were a problem with some of the first applications of linear finite elements for vertical discretization. One might expect such problems to become worse with higher order element functions, but no such problems were encountered with either second or third order elements. Fig. 14 gives the example of a vertical cross-section for a day 10 forecast obtained with cubic spline elements. No small scale noise is apparent. However, the problem remains that some of the cases required a reduced timestep, and the data assimilation run had a noisy top level. Hopefully, these problems will disappear with the introduction of a finite-element semi-implicit scheme and hybrid coordinates. Work on this is in progress.

(b) Synoptic assessment

Between days 5 and 10, significant differences between control and finite element runs develop. The synoptic examples given here are intended to indicate the sensitivity of the forecast to finite element discretization.

Fig. 15 shows 1000 mb height fields for the forecast with the quadratic finite element scheme and the control run from 10.10.84 at day 8. The main difference between the forecasts is a more realistic position of the high between 150°W and 180° with the finite element scheme. The low over the Pacific has a better amplitude in the control run, but the complex low over Europe and the Atlantic has a different structure in each forecast. Both models predict too low a pressure near 30°W. The finite element scheme produces a better representation of the trough extending along latitude 60°.

Fig. 16 shows the 500 mb field of the forecasts from 30.1.85. The main deficiency of the forecasts is the development of an artificial high near the north pole. Consequently the adjacent low fails to extend far enough north.

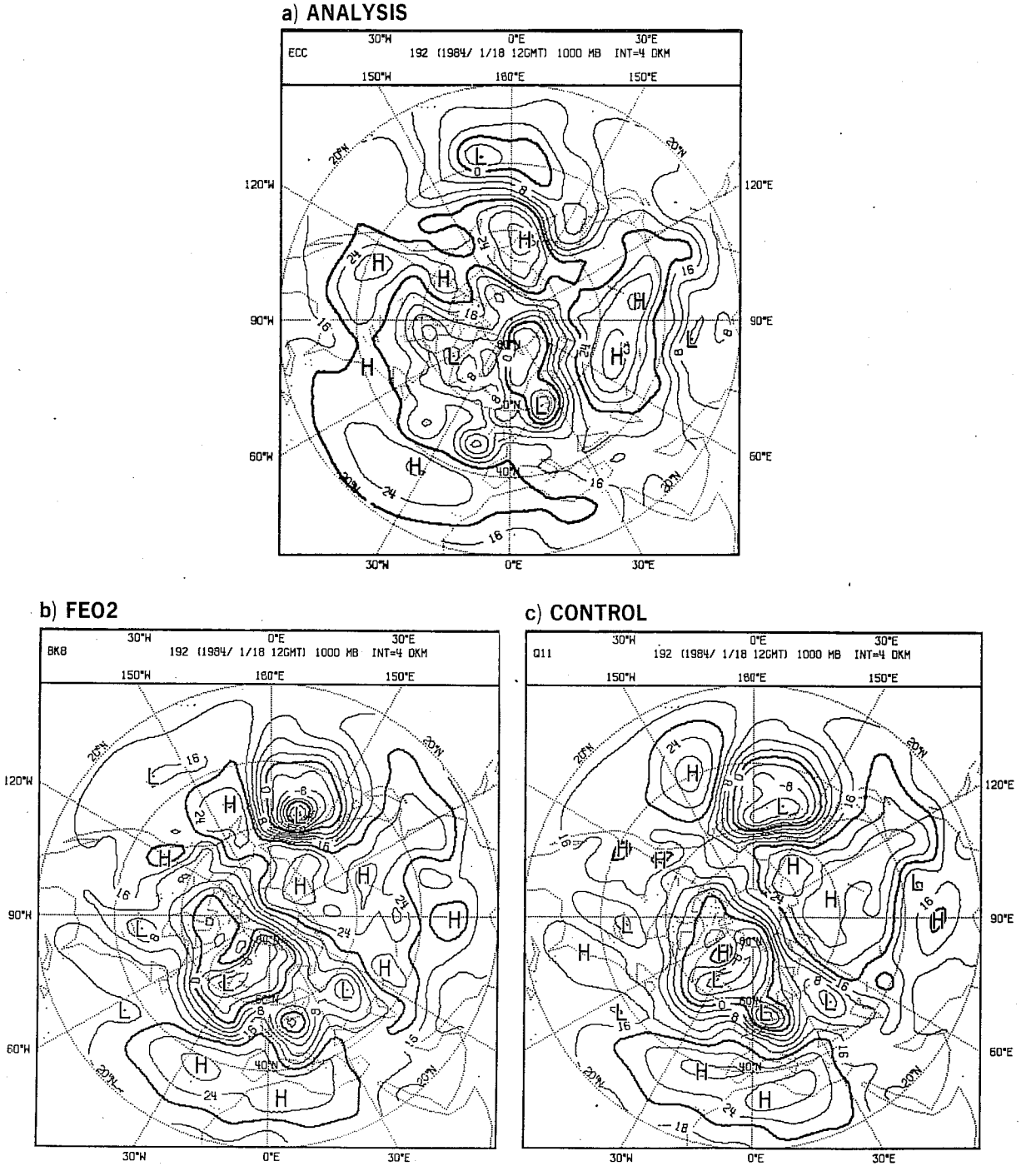

Fig. 15 D+8, 1000 mb height field for forecast from 10.1.84.

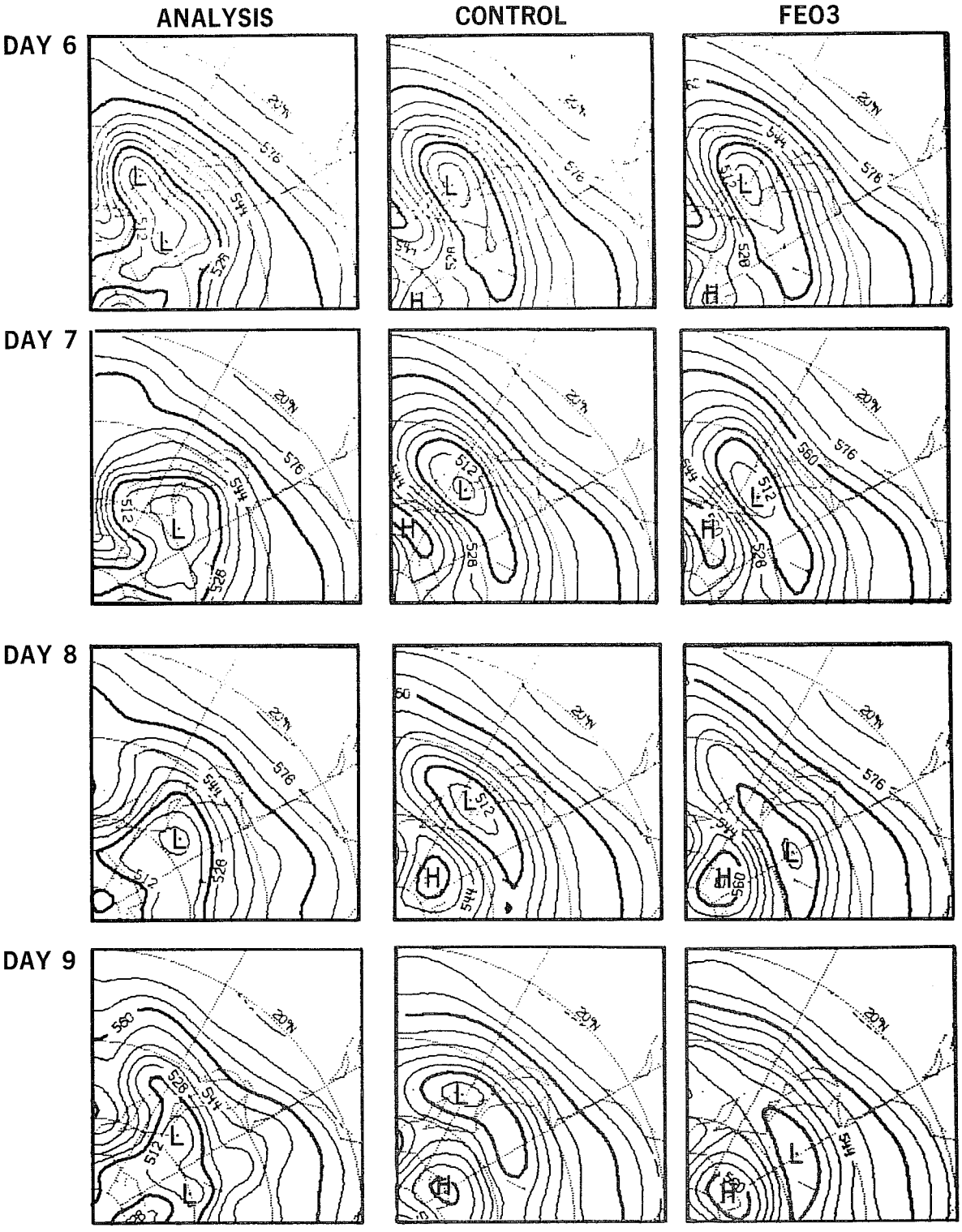

Fig. 16 Forecast from 30.1.85, 500 mb.

This low is nearly identical in the forecasts using cubic spline finite elements and finite differences at day 6. At day 8, the position of this low differs by 30° of longitude in the two forecasts. In reality, the low centre lies between the two forecast positions.

Fig. 17 shows the 1000 mb forecast from 10.1.84. In this example, the models represent some of the newly developing lows, though sometimes with considerable phase and amplitude error. In comparison with the analysis, the models tend to connect the different lows, producing too few centres and making such centres not distinct enough. The cubic spline scheme somewhat reduces this error, reaching at day 9 a state with more distinct lows and producing a new low at 0°E, though misplacing this low over Italy instead of over northern France.

Fig. 18 shows the 1000 mb fields of day 5 forecasts from 20.1.85; the forecasts are still very similar. For the complex low between 60°W and 60°E a tendency of the finite element schemes to produce slightly more pronounced separate lows can already be seen.

The rainfall patterns are very similar for the finite element and control runs. However, the amplitudes differ by up to 20%.

Fig. 19 shows the zonal kinetic energy for the control and cubic spline finite element runs, averaged zonally and for days 5 to 10. The amplitude of the jet stream is slightly underpredicted with the third order finite elements, but the amplitude is better than in the control. For the other cases the amplitudes of the jet stream are listed in Table 4. In most cases, the amplitude of the jet in the control run is too small. Overall the third order elements give a better amplitude.

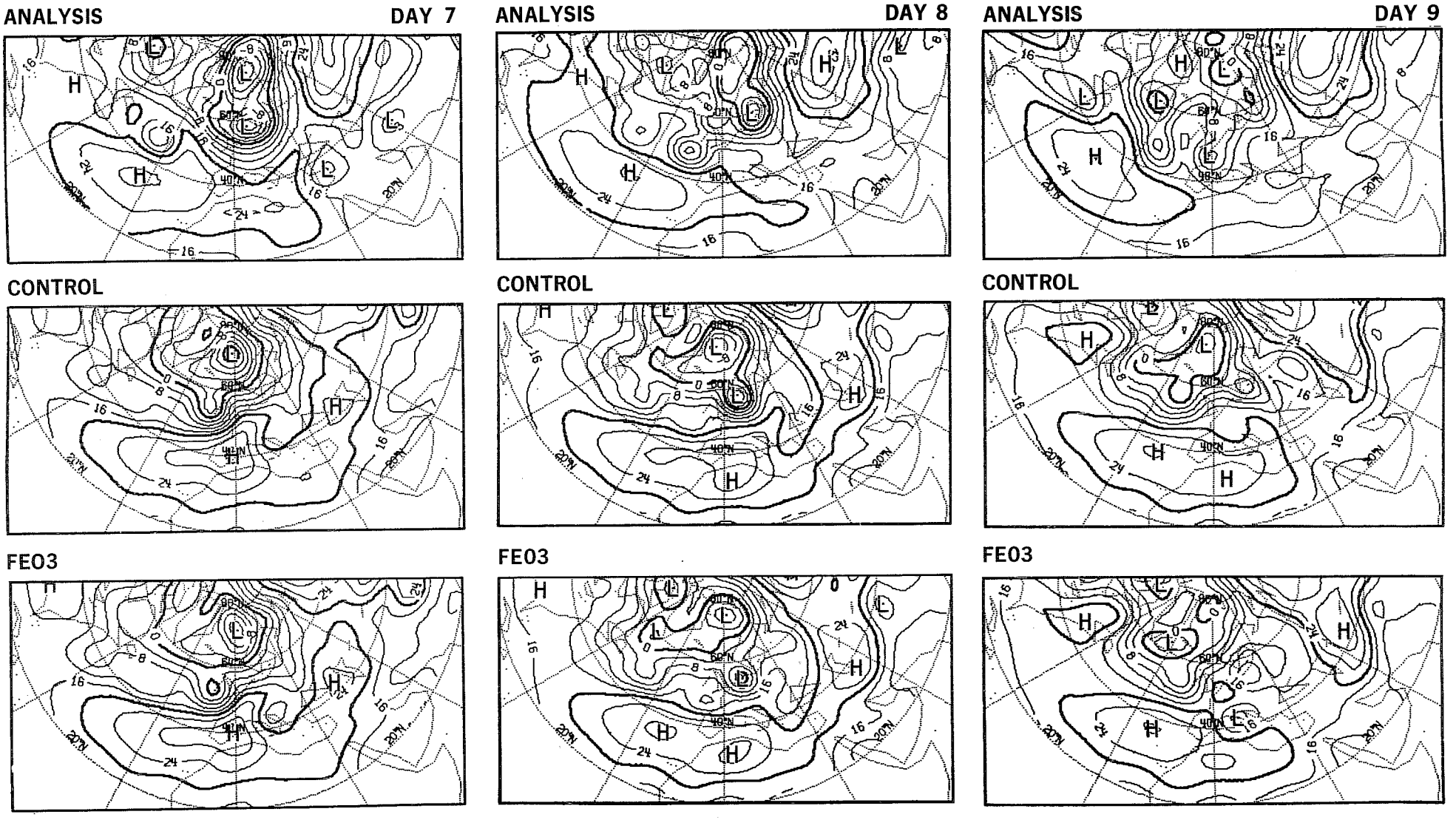

Fig. 17 Forecast from 10.1.84, 1000 mb.

ANALYSIS

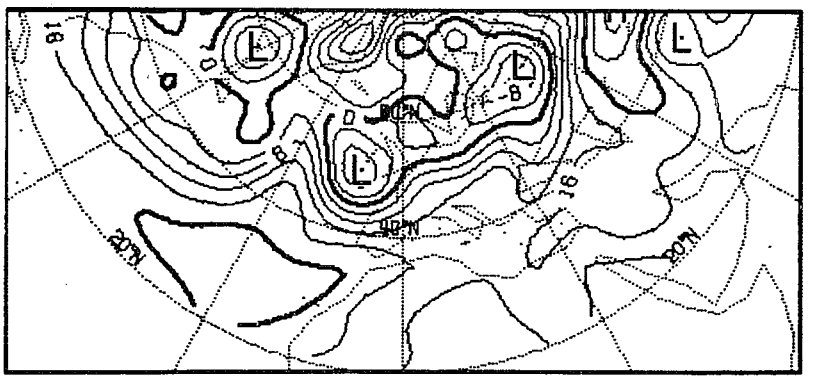

CONTROL

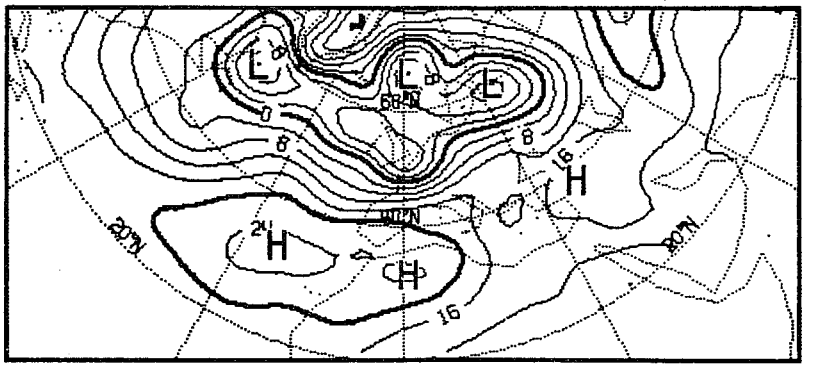

FE02

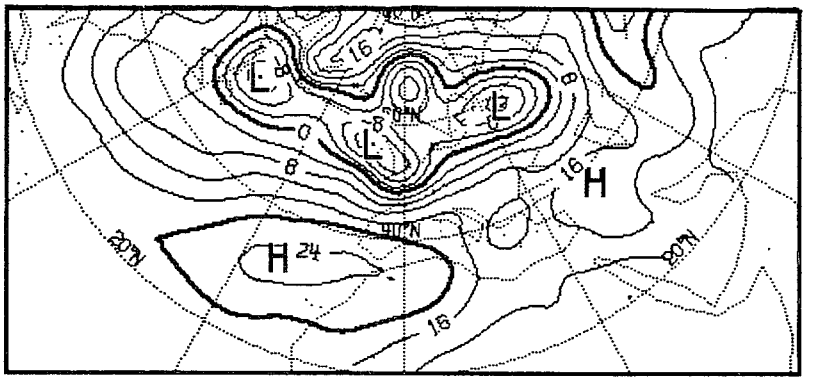

FE03

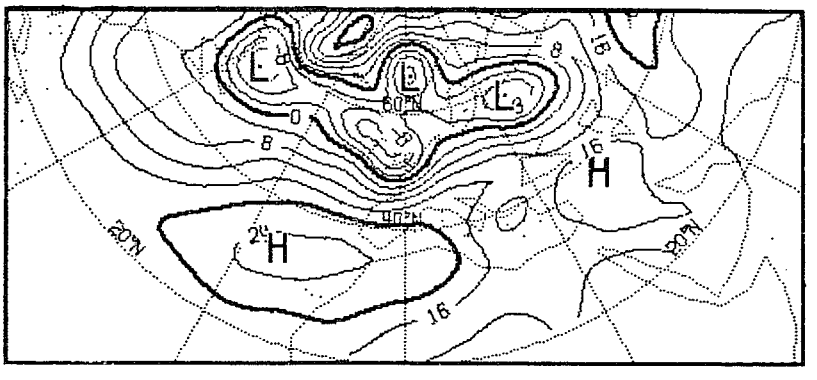

Fig. 18 D5 forecast from 20.1.85, 1000 mb.

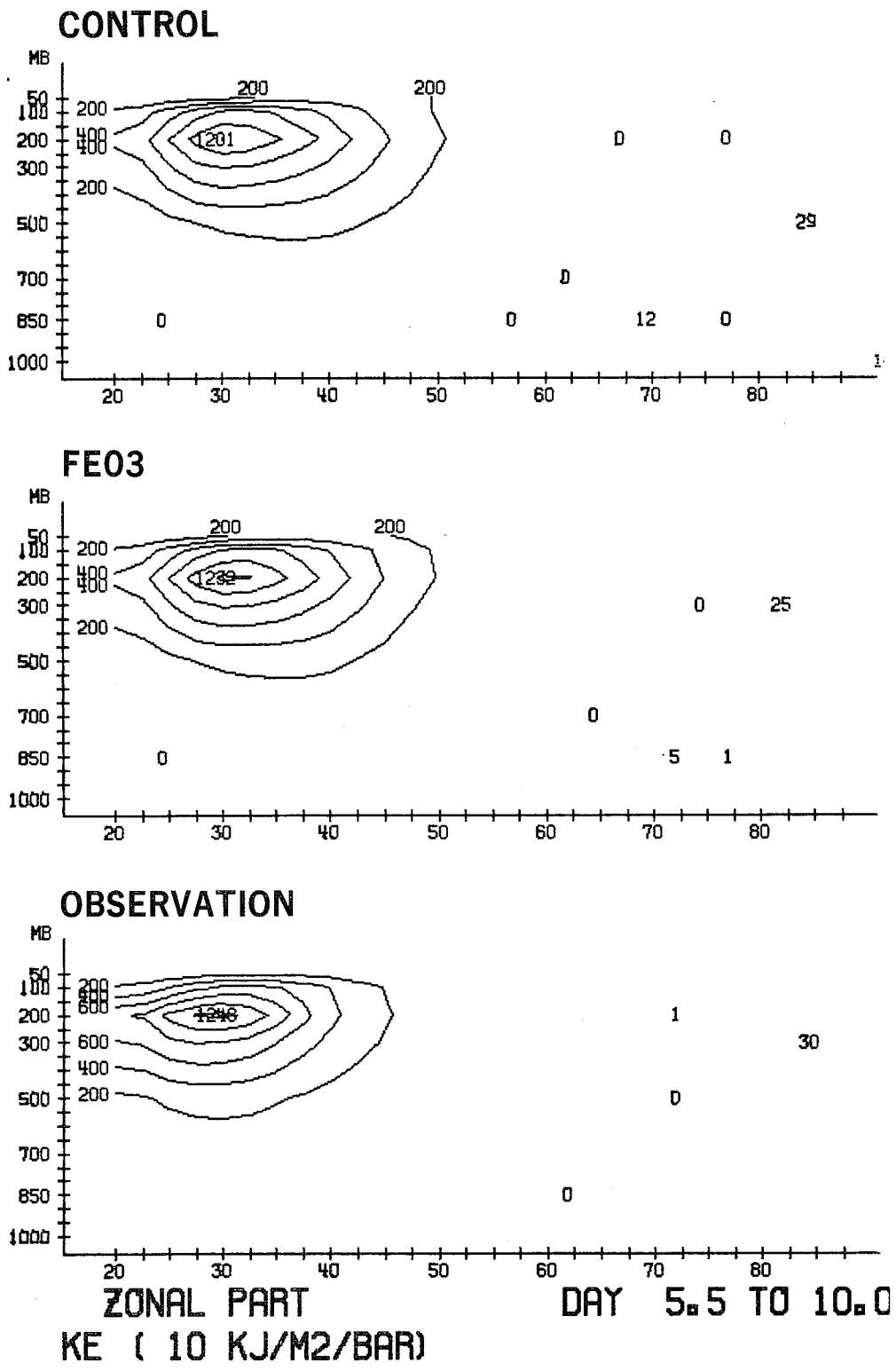

Fig. 19 Zonally averaged zonal kinetic energy for forecast from 10.1.85.

Amplitude of jet stream
[10 kJ/m^2 bar]

Case No.	Observed	Control	Cubic Splines
1	1347	1047	1105
2	1285	1315	1291
3	1248	1201	1232
4	1251	1088	1131
5	1085	907	897
6	1063	889	933
rms difference to observation		71	59

Table 4 Amplitude of main maximum of normal kinetic energy

In order to compare the performance of models with high and low order element functions, three forecasts were performed using linear elements and applying the same simplification at the boundary as employed with the cubic spline elements. Fig. 20a shows a comparison of these with the control runs. On average, no improvement is encountered with the first order finite elements. This is in contradiction with the results of Burridge et al. (1985), but may be due to the simplified boundary treatment employed. Fig. 21 gives a further indication of this, showing the forecast error of temperature. An increased forecast error is encountered due to the simplified treatment of the top boundary with linear elements. In comparison, there seems to be less sensitivity to a bad treatment of the top boundary with cubic spline elements.

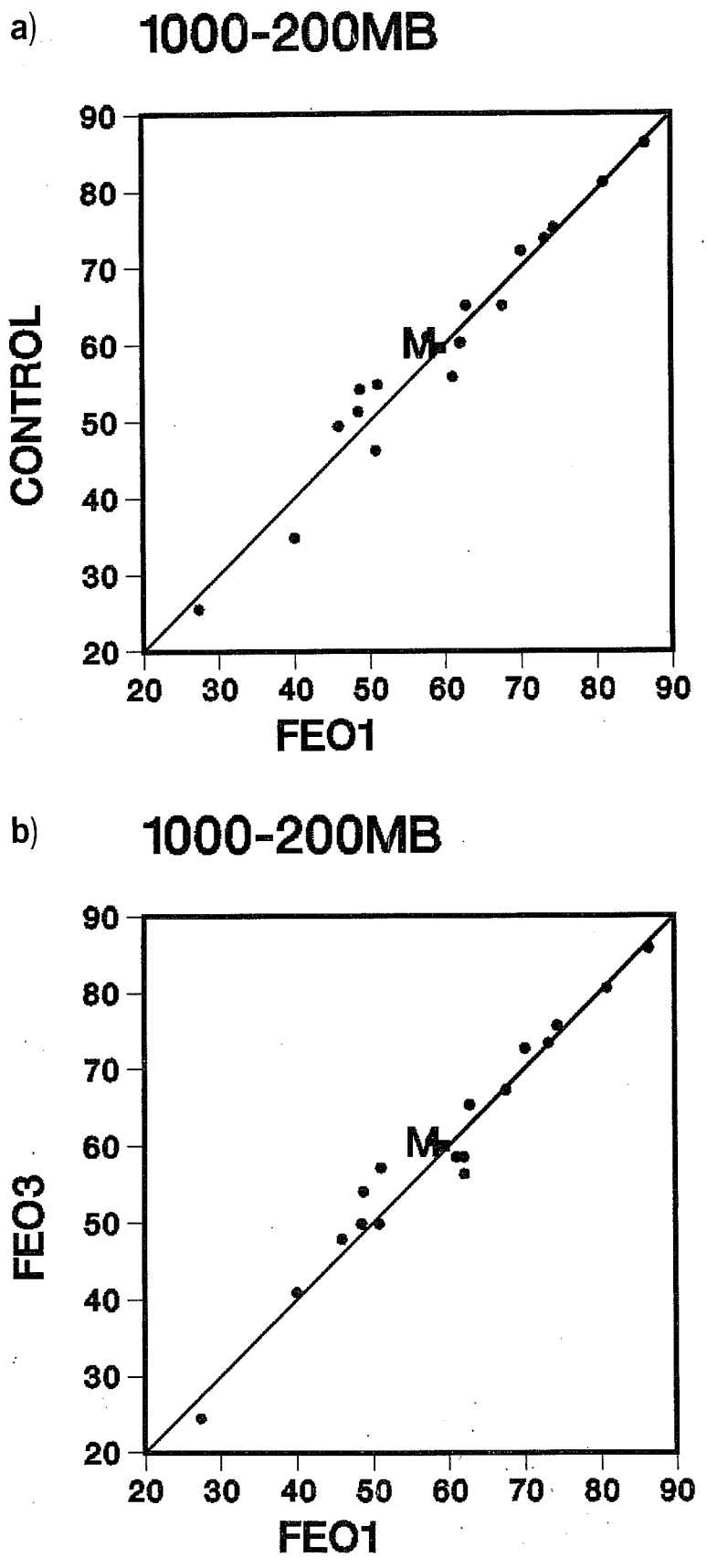

Fig. 20 Total anomaly correlations of height, 1000-200 mb, scatter diagram (a) comparing control run and first order finite element scheme with simplified boundary treatment for cases 2,3,6 of set 2, and (b) the corresponding results comparing the first and third order schemes.

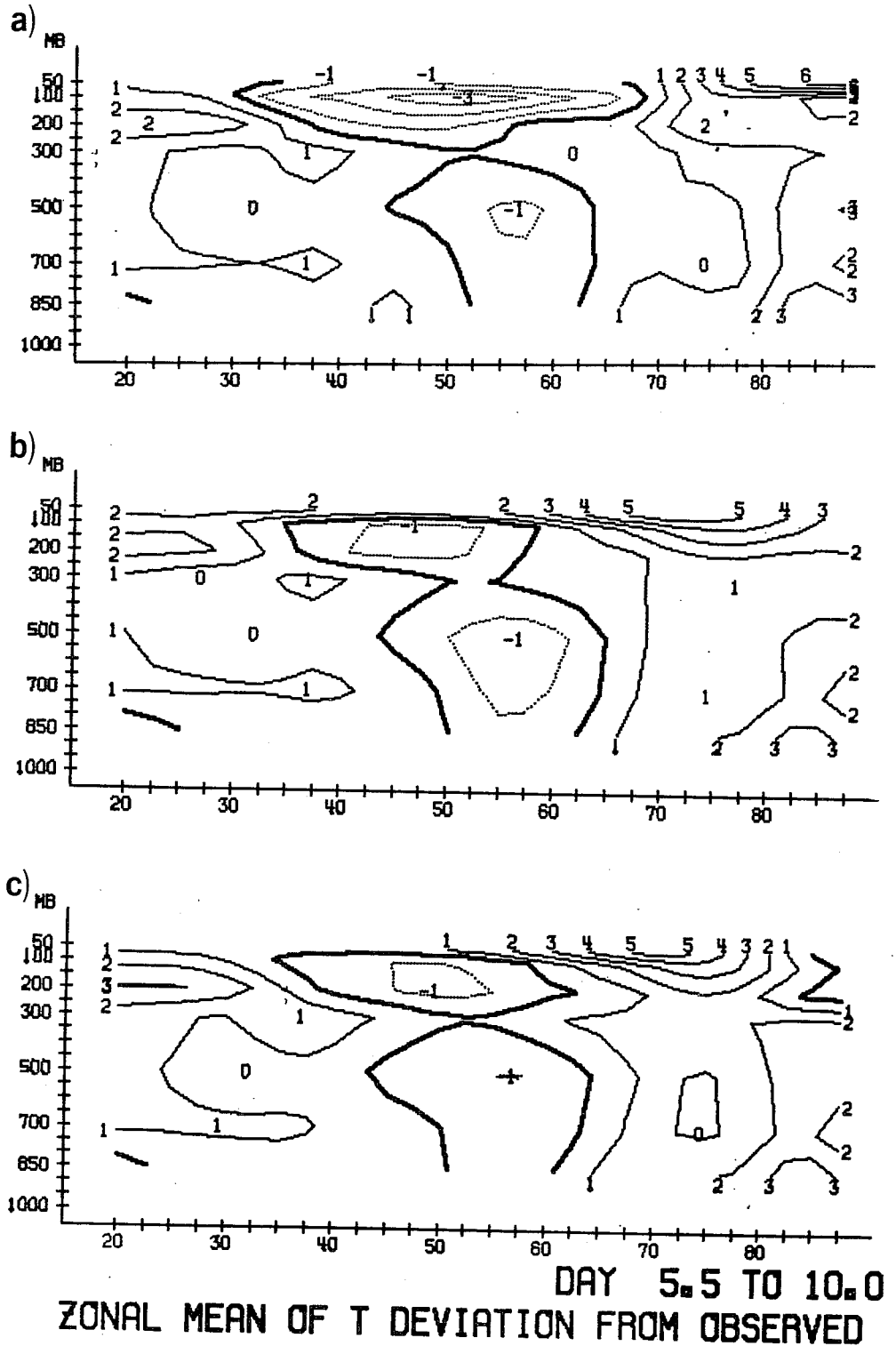

Fig. 21 Temperature errors for forecast from 10.1.85, averaged zonally and in time. (a) linear elements; (b) control; (c) cubic spline elements.

For cubic splines, the temperature error is comparable to that of the control run. Fig. 20b shows the comparison of linear and cubic spline elements. An advantage of the cubic elements over the linear ones can be seen. In view of the small sample and the simplified boundary treatment, however, a final decision between these two schemes cannot be made at this point.

4.3 50 day integrations

According to Burridge et al. (1985), the finite element discretization and the treatment of the top boundary has a substantial influence on the climate properties of the model. Here, we investigated only the climate properties of the quadratic elements, since the cubic elements are available only with a simplified boundary treatment.

50 day integrations with resolution T42 and initial date 17.1.84 were done using quadratic elements with boundary treatments B0 and B4 described in Section 2.4 of Burridge et al. 1985. Fig. 22 shows time averaged 500 mb fields (day 25 to 50) for analysis, control run, and quadratic finite elements with the two boundary treatments.

As in the experiments with linear elements, reported in Burridge et al. (1985), the form and position of the polar low is better for the finite element runs. The ridge at 120°W and trough at 150°W are very weak with the B0 boundary, but these features are rather exaggerated with boundary B4. However the phase of the ridge in both these cases is now nearly correct and is also improved compared with the linear elements given in Burridge et al. (1985).

A further improvement is a better position of the centre of the low near 60°W which is also improved in comparison with the linear elements.

Fig. 23 shows the zonally averaged temperature errors. There is a strong temperature error at the top of the atmosphere. The model with quadratic elements and boundary B4 reduces this error and the gradient at the top model level.

The kinetic energy of the zonal mean flow averaged over days 25 to 50 is shown in Fig. 24. The finite elements with boundary B4 have an improved amplitude of the subtropical jet stream, and the high velocities at the top of the atmosphere are reduced; the position of the subtropical jet is also slightly improved. However the strength of the stratopsheric jet can be very variable because of sudden warmings and related events. Therefore a large sampling error may be encountered in this respect.

Fig. 25 shows the spectrum of kinetic energy. For the shorter wavelengths, the quadratic elements produce the more realistic spectrum, though it is worse for wavenumbers 1 and 2.

a) ANALYSIS

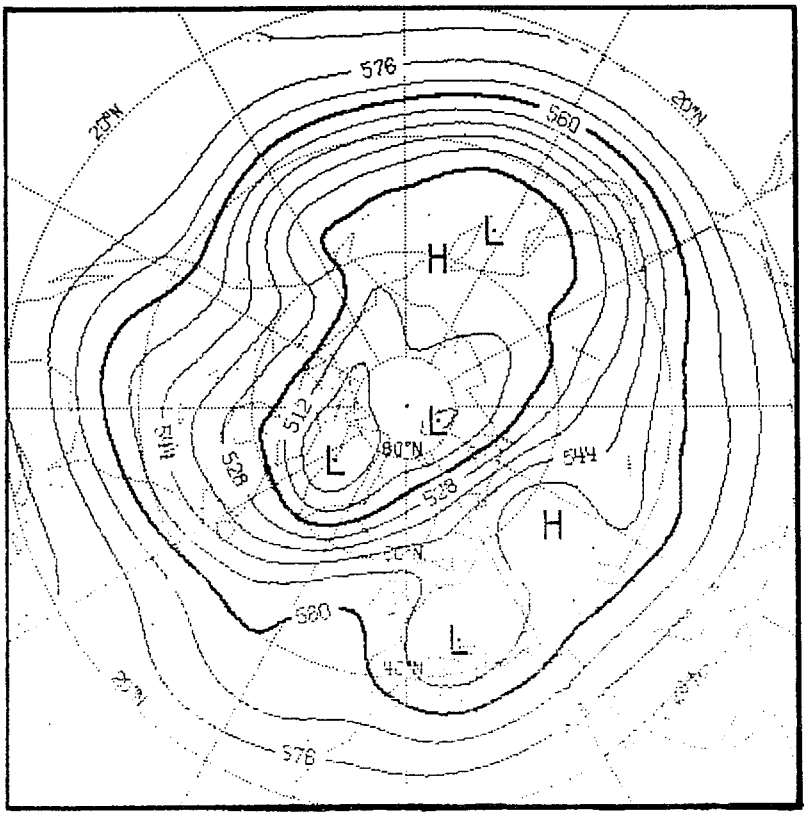

b) CONTROL

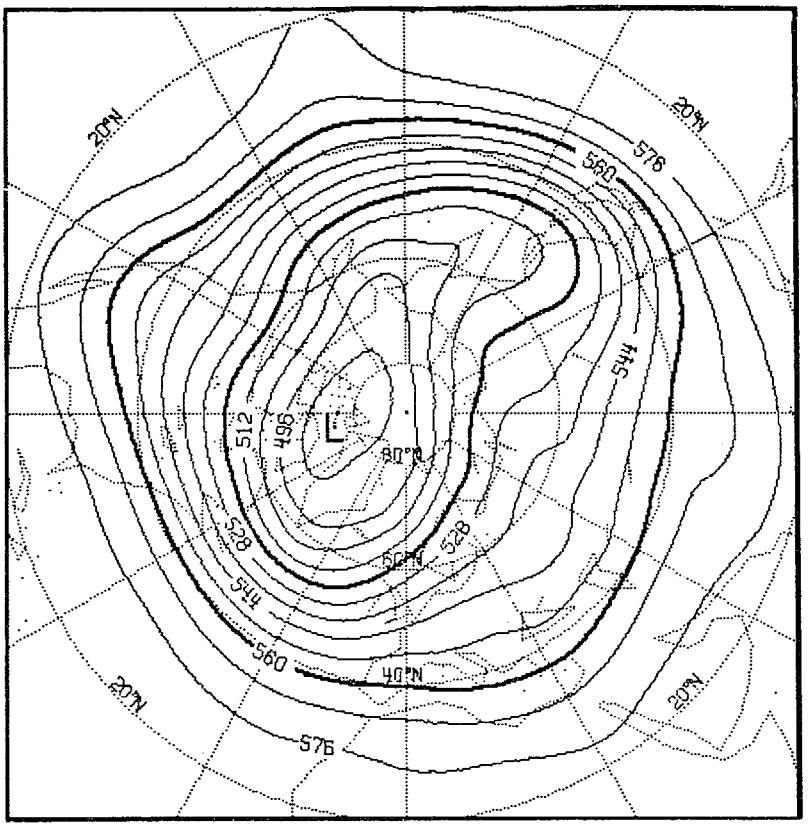

Fig. 22 50 day runs, time averaged fields day 25 to 50.

c) FE02, BO

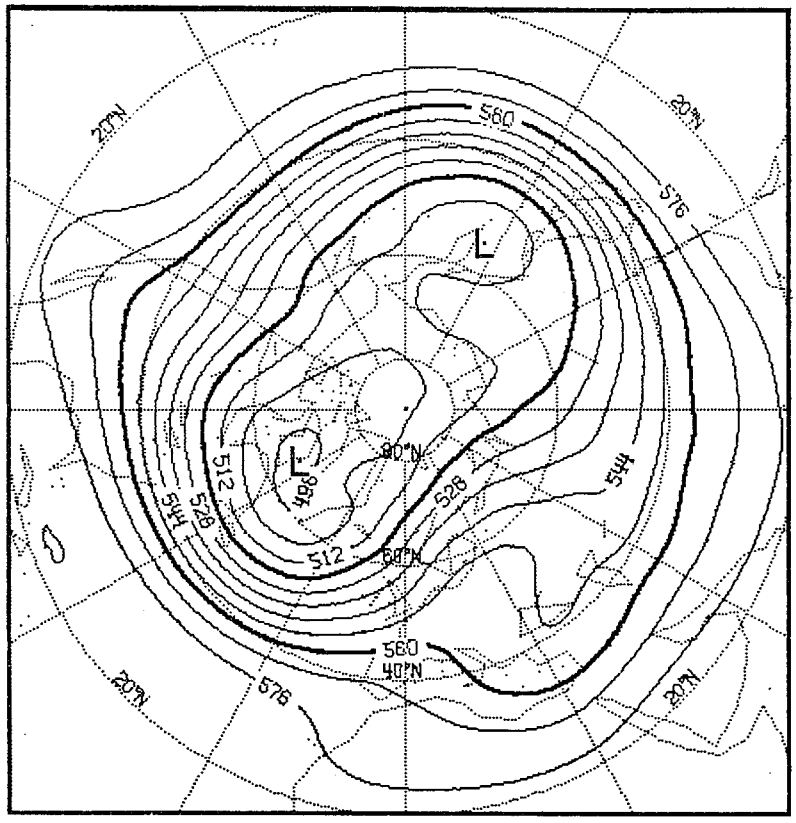

d) FE02, B4

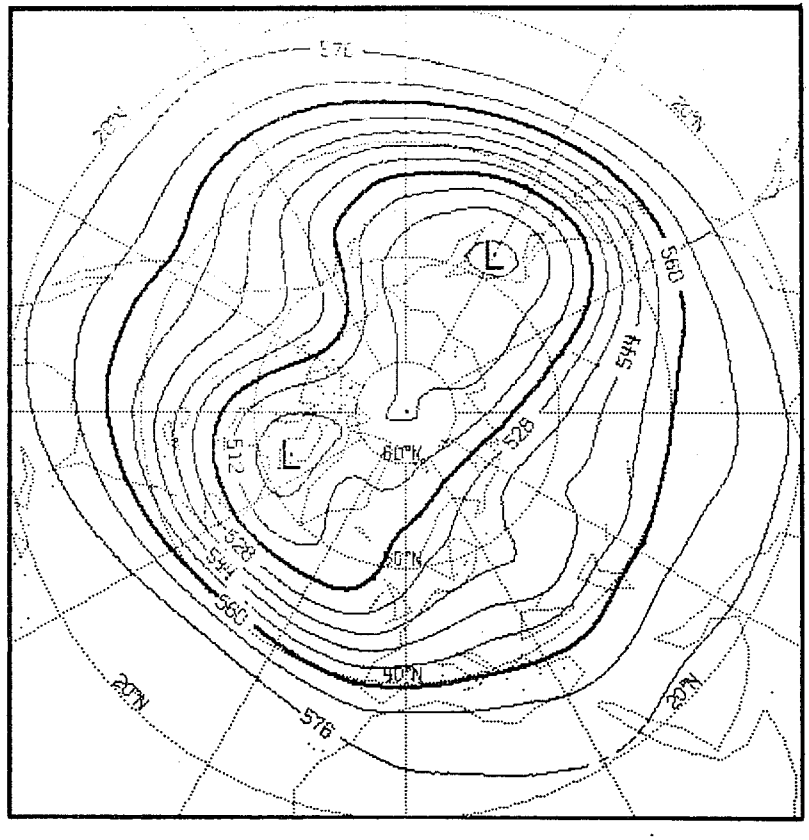

Fig. 22 Continued

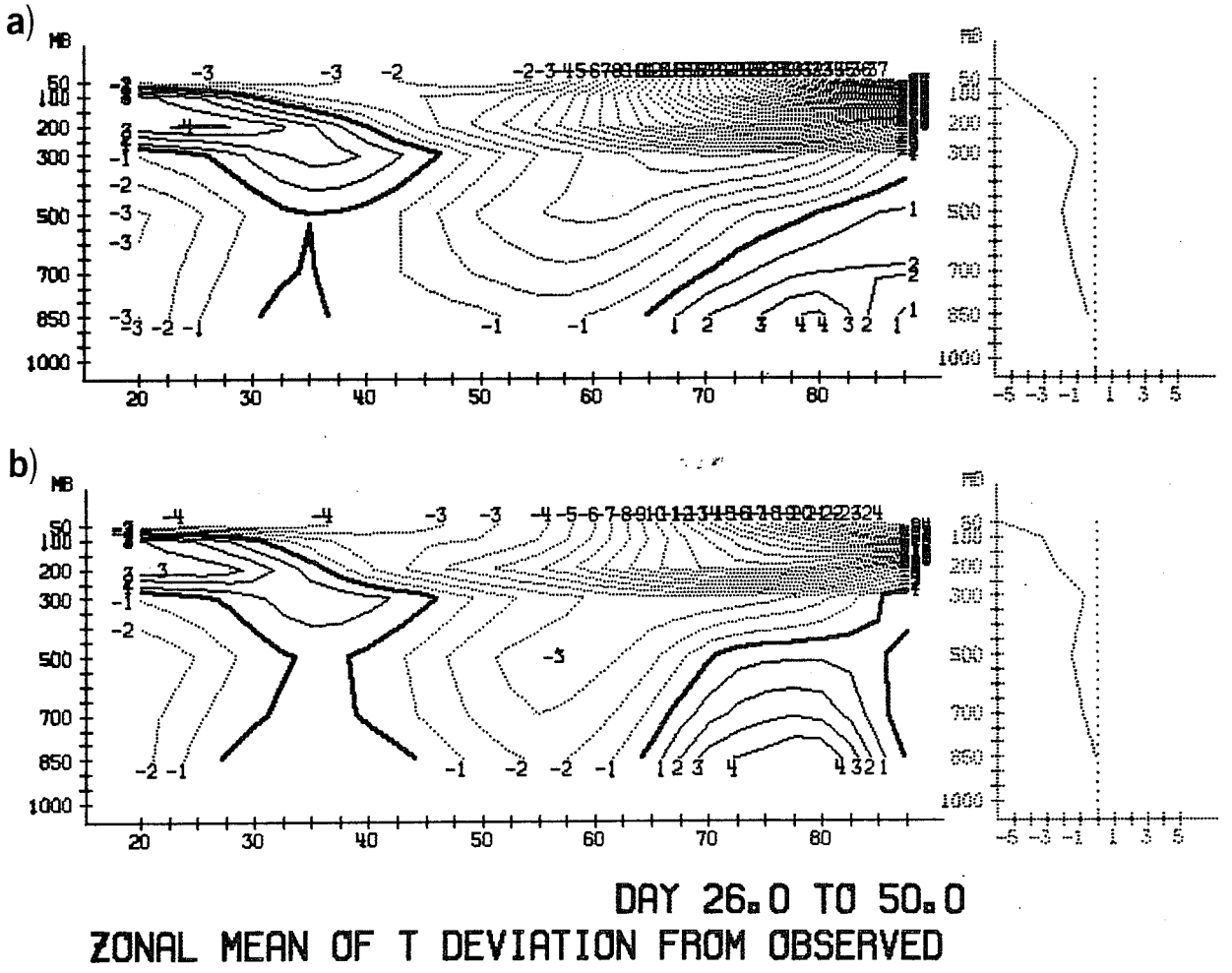

Fig. 23 Zonally averaged temperature error. (a) control run; (b) finite elements, order 2, boundary 4.

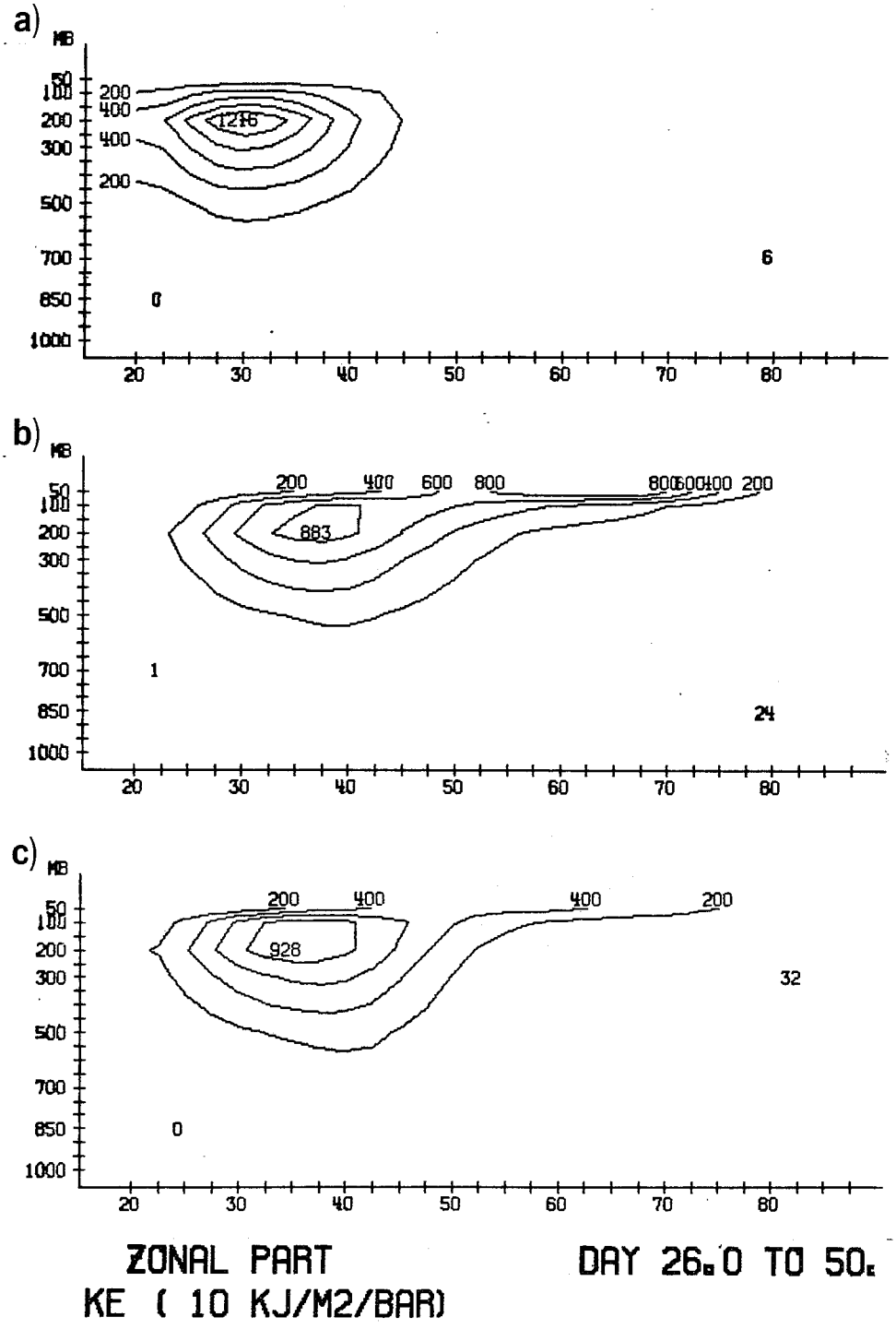

Fig. 24 Zonal kinetic energy. (a) observation; (b) control run; (c) finite elements, order 2, boundary 4.

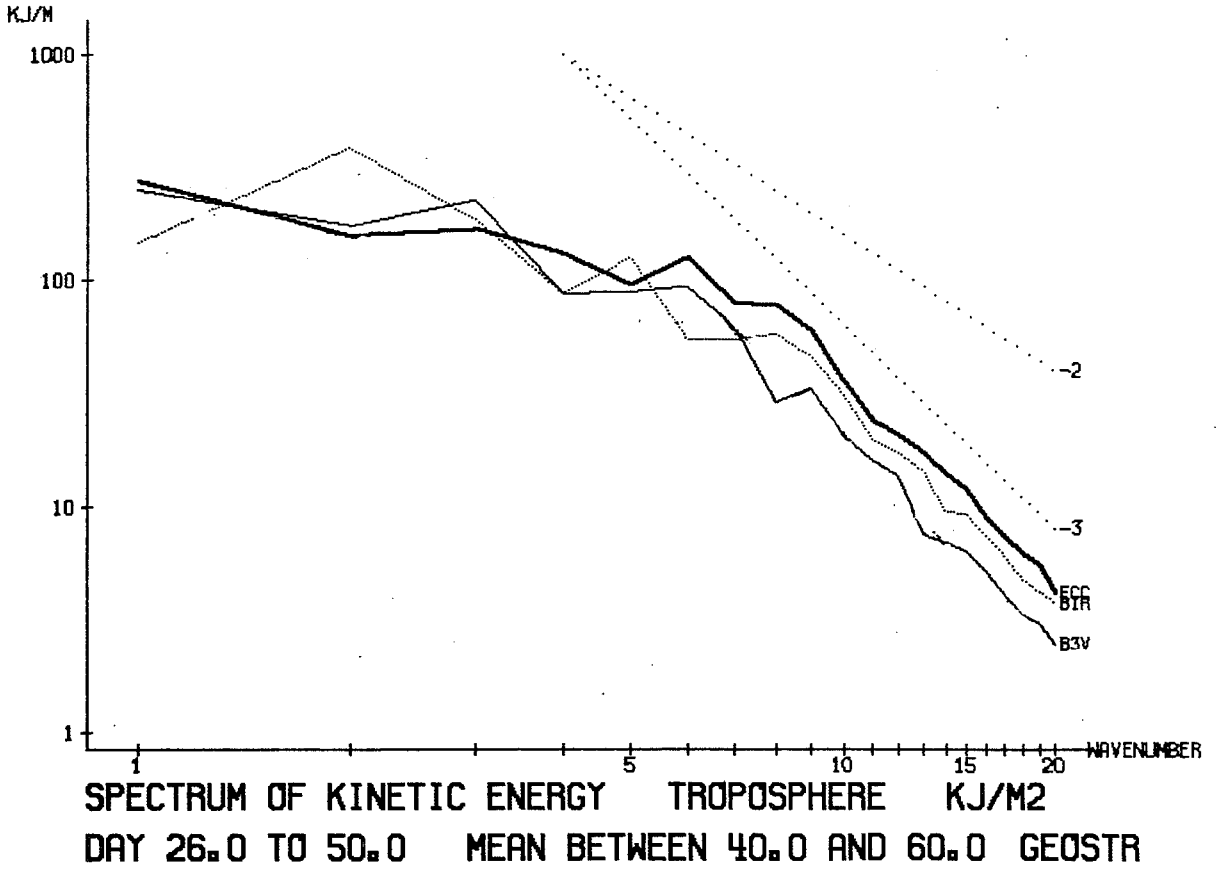

Fig. 25 Spectrum of kinetic energy, thick line = observation, thin solid line=control run, dotted line = finite elements, order 2, boundary 4.

5. CONCLUSIONS

Vertical finite element schemes with basis functions of order 2 and 3 have been implemented with the ECMWF spectral model. Different ways of implementing the full Galerkin treatement were examined in order to find the most efficient implementation. The second order elements are computationally not more expensive than the linear elements, but the cubic spline elements are more expensive.

In this study, no attempt is made to achieve more computational efficiency by using simplifications of the Galerkin scheme, for example by using fewer collocation points or treating some fields by linear, others by cubic spline in an energy conserving way. For a possible operational implementation of the cubic spline scheme, the investigation of such simplifications may be of importance.

Even though the third order scheme was implemented only with a simplified top boundary treatment, both the second and third order scheme resulted in a systematic improvement over the control runs in 10-day forecasts. A systematic relationship between second and first order elements or second and third order elements was not found; these schemes improved different cases. There is a tendency for the finite element models to increase the amplitude of the shorter scales.

To investigate the relation between cubic spline and linear elements, three forecasts were done with linear elements, using the same simplification at the top, as employed with the cubic spline elements. For these cases, the cubic spline elements performed better. However, to decide finally between these methods a larger sample has to be used, and a proper boundary treatment has to be employed.

Starting from operational ECMWF analyses, relevant differences to the control run appear near day 5. Using the finite element scheme in the analysis cycle, however, results in a reduction of the first guess error already after 12 h.

50 day integrations with the second order scheme confirmed that the finite element schemes have some potential for improving the climate properties of models. The climate properties of the model are also very much dependent on the treatment of the top level, which according to Burridge et al. is also very much the case for the gridpoint version of the model.

References

Ahlberg, J.H., E-N. Nilson, and J.L. Walsh, 1967: The theory of splines and their applications. Academic Press, New York, 284 pp.

Burridge, D.M., J. Steppler, R. Strüfing, 1985: Finite elment schemes for the vertical discretization of the ECMWF forecast model using linear elements, ECMWF Tech.Rep.No.54, 48 pp.

Gallagher, R.H., O.C. Zienkiewicz, J.T. Oden, M. Morandi Cecchi, and C. Taylor, 1978: Finite elements in fluids, Volume 3. Wiley and Sons, Chichester, 396 pp.

Girard, C. and M. Jarraud, 1982: Short and medium forecast differences between a spectral and grid point model. An extensive quadi operational comparison. ECMWF Tech.Rep.No.32, 178 pp.

Kreiss, H.O. and J. Oliger, 1972: Comparison of accurate methods for the integration of hyperbolic equations. Tellus, 24, 199-215.

Louis, J.F., 1984: ECMWF forecasting model: adiabatic part. ECMWF Research Manual 2 (Met. Bulletin M1.6/2).

Staniforth, A.N., and R.W. Daley, 1977: A finite-element formulation for the vertical discretization of sigma coordinate primitive equation models. Mon.Wea.Rev., 105, 1108-1118.

Steppeler, J., 1975: On a high accuracy finite difference scheme. J.Comp.Phys., 19, 390.

Steppeler, J., 1976a: The application of the second and third degree methods. J.Comp.Phys., 22, 295-318.

Steppeler, J., 1976b: A baroclinic model using a high accuracy horizontal discretization. Contrib.Atmos.Phys., 49, 285-298.

ECMWF PUBLISHED TECHNICAL REPORTS

No.1 A Case Study of a Ten Day Prediction

No.2 The Effect of Arithmetic Precisions on some Meteorological Integrations

No.3 Mixed-Radix Fast Fourier Transforms without Reordering

No.4 A Model for Medium-Range Weather Forecasting - Adiabatic Formulation

No.5 A Study of some Parameterizations of Sub-Grid Processes in a Baroclinic Wave in a Two-Dimensional Model

No.6 The ECMWF Analysis and Data Assimilation Scheme - Analysis of Mass and Wind Fields

No.7 A Ten Day High Resolution Non-Adiabatic Spectral Integration: A Comparative Study

No.8 On the Asymptotic Behaviour of Simple Stochastic-Dynamic Systems

No.9 On Balance Requirements as Initial Conditions

No.10 ECMWF Model - Parameterization of Sub-Grid Processes

No.11 Normal Mode Initialization for a Multi-Level Gridpoint Model

No.12 Data Assimilation Experiments

No.13 Comparisons of Medium Range Forecasts made with two Parameterization Schemes

No.14 On Initial Conditions for Non-Hydrostatic Models

No.15 Adiabatic Formulation and Organization of ECMWF's Spectral Model

No.16 Model Studies of a Developing Boundary Layer over the Ocean

No.17 The Response of a Global Barotropic Model to Forcing by Large-Scale Orography

No.18 Confidence Limits for Verification and Energetic Studies

No.19 A Low Order Barotropic Model on the Sphere with the Orographic and Newtonian Forcing

No.20 A Review of the Normal Mode Initialization Method

No.21 The Adjoint Equation Technique Applied to Meteorological Problems

No.22 The Use of Empirical Methods for Mesoscale Pressure Forecasts

No.23 Comparison of Medium Range Forecasts made with Models using Spectral or Finite Difference Techniques in the Horizontal

No.24 On the Average Errors of an Ensemble of Forecasts

ECMWF PUBLISHED TECHNICAL REPORTS

No.25 On the Atmospheric Factors Affecting the Levantine Sea

No.26 Tropical Influences on Stationary Wave Motion in Middle and High Latitudes

No.27 The Energy Budgets in North America, North Atlantic and Europe Based on ECMWF Analyses and Forecasts

No.28 An Energy and Angular-Momentum Conserving Vertical Finite-Difference Scheme, Hybrid Coordinates, and Medium-Range Weather Prediction

No.29 Orographic Influences on Mediterranean Lee Cyclogenesis and European Blocking in a Global Numerical Model

No.30 Review and Re-assessment of ECNET - a Private Network with Open Architecture

No.31 An Investigation of the Impact at Middle and High Latitudes of Tropical Forecast Errors

No.32 Short and Medium Range Forecast Differences between a Spectral and Grid Point Model. An Extensive Quasi-Operational Comparison

No.33 Numerical Simulations of a Case of Blocking: the Effects of Orography and Land-Sea Contrast

No.34 The Impact of Cloud Track Wind Data on Global Analyses and Medium Range Forecasts

No.35 Energy Budget Calculations at ECMWF: Part I: Analyses

No.36 Operational Verification of ECMWF Forecast Fields and Results for 1980-1981

No.37 High Resolution Experiments with the ECMWF Model: a Case Study

No.38 The Response of the ECMWF Global Model to the El-Nino Anomaly in Extended Range Prediction Experiments

No.39 On the Parameterization of Vertical Diffusion in Large-Scale Atmospheric Models

No.40 Spectral characteristics of the ECMWF Objective Analysis System

No.41 Systematic Errors in the Baroclinic Waves of the ECMWF Model

No.42 On Long Stationary and Transient Atmospheric Waves

No.43 A New Convective Adjustment Scheme

No.44 Numerical Experiments on the Simulation of the 1979 Asian Summer Monsoon

No.45 The Effect of Mechanical Forcing on the Formation of a Mesoscale Vortex

ECMWF PUBLISHED TECHNICAL REPORTS

No.46 Cloud Prediction in the ECMWF Model

No.47 Impact of Aircraft Wind Data on ECMWF Analyses and Forecasts during the FGGE Period, 8-19 November 1979 (not on WP, text provided by Baede)

No.48 A Numerical Case Study of East Asian Coastal Cyclogenesis

No.49 A Study of the Predictability of the ECMWF Operational Forecast Model in the Tropics

No.50 On the Development of Orographic Cyclones

No.51 Climatology and Systematic Error of Rainfall Forecasts at ECMWF

No.52 Impact of Modified Physical Processes on the Tropical Simulation in the ECMWF Model

No.53 On the Performance and Systematic Errors of the ECMWF Tropical Forecasts (1982-1984)

No.54 Finite Element Schemes for the Vertical Discretization of the ECMWF Forecast Model Using Linear Elements

No.55 Finite Element Schemes for the Vertical Discretization of the ECMWF Forecast Model using Quadratic and Cubic Elements